# Meteorological tsunami generation due to sea-surface pressure change: Three-dimensional theory and synthetics of ocean-bottom pressure change

**Tatsuhiko Saito[1], Tatsuya Kubota[1], Notaka Y. Chikasada[1], Yuusuke Tanaka[2], and Osamu Sandanbata[1]**

[1]National Research Institute for Earth Science and Disaster Resilience, Tsukuba, Japan.

[2]Japan Agency for Marine-Earth Science and Technology, Yokohama, Japan.

Corresponding author: Tatsuhiko Saito (saito-ta@bosai.go.jp)
ORCID: 0000-0003-1188-9223

Running Title: 3-D METEOROLOGICAL TSUNAMI GENERATION

**Key Points:**

- 3-D solutions describing the tsunami generation due to sea-surface pressure change are derived.
- The solutions can simulate ocean-bottom pressure changes during the generation that are detectable by recent open-ocean array observations.
- Short-wavelength dispersive tsunamis can be enlarged more by a moving pressure change source, compared with long-wavelength tsunamis.

## Abstract

Although most tsunamis are generated by the sea-bottom deformation caused by earthquakes, some tsunamis are excited by sea-surface pressure changes. This study theoretically investigated tsunamis generated by sea-surface pressure changes and derived the solutions in 3-D space, whereas most past studies employed 2-D equations. Using the solutions, we simulated and visualized the tsunami generation by a growing pressure change. Negative pressure change made the sea surface uplifted inside the source region and negative leading waves were radiated from the source region. We also simulated the tsunami generation when the pressure change at the sea surface moves with almost the same speed as the tsunami propagation velocity. The tsunami height increased with increasing the travel distance including the dispersion effects. The 3-D solutions in this study, including the vertical velocity distribution, indicate that both the tsunami height and the sea-surface pressure changes contribute to the ocean-bottom pressure changes, suggesting the difficulty in measuring the tsunami height with ocean-bottom pressure observations. When the pressure change source was characterized by short-wavelength components, the dispersion increased tsunami height more extensively than the non-dispersive tsunamis. The 3-D solutions are necessary for describing the tsunami generation where the long-wave approximations are not applicable in open oceans.



## Plain Language Summary

Although most tsunamis are generated by giant earthquakes, some tsunamis are excited by meteorological phenomena such as storms and moveing convective system, which are known as meteorological tsunamis or meteotsunamis. Most studies employ 2-D equations for modeling meteorological tsunamis. This is mainly because past studies used coastal records that cannot directly observe tsunami generation. However, recent tsunami sensors have enabled us to capture the tsunamis in open oceans and we expect that they can directly observe the generation. In order to fully investigate the generation process including vertical water flow, the theory needs to be formulated in the 3-D space. This study theoretically formulate meteorological tsunamis in the 3-D space. We derive new solutions that can theoretically visualize the tsunami generation and growing processes. The solutions also predict the pressure changes at the sea bottom during the generation, which are observable by recent tsunami observation networks.


## 1 Introduction

While disastrous tsunamis are mostly generated by large earthquakes, some tsunamis are excited by pressure disturbances at sea surfaces caused by meteorological phenomena such as storms and moving convective systems (e.g., Churchill et al. 1995; Monserrat et al. 2006). Such tsunamis are known as meteorological tsunamis or meteotsunamis. The basic generation mechanism of a meteorological tsunami was theoretically investigated in 2-D space with long-wave approximations (e.g., Proudman 1929; Greenspan 1956; An et al. 2012; Seo & Liu 2014). These studies predicted that the sea-surface pressure change moving at nearly the same speed as the tsunami speed efficiently amplifies the tsunami height. This amplification is often called the Proudman effect. Meteorological tsunamis have been observed in different regions in the world (e.g., Šepić et al. 2015; Rabinovich et al. 2020). Numerous studies analyzed the records using tsunami simulations reproducing the Proudman effect (e.g., Hibiya & Kajiura 1982). For

example, Hibiya & Kajiura (1982) analyzed tide gauge records of meteorological tsunamis observed in Nagasaki bay, Japan. They numerically simulated records by setting a moving pressure change at the sea surface as a force in the long-wave equations. Using detailed distribution of meteorological data such as atmospheric pressure distributions and wind speed distributions, researchers have investigated the sources of meteorological tsunamis (e.g., Williams et al. 2019; Heidarzadeh et al. 2020).

Those analyzed tsunami records were mostly observed near coasts with eyewitness, video captures, and tide gauge records (e.g., Heidarzadeh et al. 2020). The tide gauge records have played an important role for quantitative analyses for the estimation of the tsunami source kinematics or excitation. However, since tide gauges are installed inside bays and harbors, the records are considerably contaminated by strong coastal site effects, which prevents from extracting the details of the generation process. Besides, because the tide gauges are located in very shallow sea and the sampling rate is too low to resolve short-period tsunamis, they hardly capture tsunami dispersion (e.g., Kubota et al. 2020a). Therefore, most past studies used the 2-D non-dispersive tsunami equations for the analyses of the observed data.

Tsunami observations have exhibited impressive growth for past decades due to the development of ocean-bottom pressure gauges, which enabled us to observe tsunamis outside bays and harbors (e.g., Bernard & Meinig 2011; Mungov et al. 2013; Tsushima & Ohta 2014; Rabinovich & Eblé 2015; Kaneda et al. 2015; Kawaguchi et al. 2015; Kanazawa et al. 2016; Aoi et al. 2020). Unlike coastal tide gauges, deep-ocean observations can capture clear tsunami signals (e.g., Grilli et al. 2013; Inazu & Saito 2014; Sandanbata et al. 2018; Kubota et al. 2020b). The high-quality records in open oceans have driven the studies about the dispersion and high-resolution tsunami source estimations (e.g., Kirby et al. 2013; Baba et al. 2015; Saito & Kubota 2020). Moreover, the ocean-bottom pressure gauges can catch the tsunamis inside the generation field (e.g., Mikada et al. 2006; Nosov et al. 2007; Mizutani et al. 2020). This drastically changed tsunami research because the generation cannot be described by the 2-D equations that were often used in past tsunami studies. The 3-D fluid theories play a fundamental role for the generation process (Takahashi 1942; Maeda et al. 2013; Lotto & Dunham 2015; Lotto et al. 2017). Saito (2013) investigated the 3-D tsunami generation due to the sea-bottom deformation, providing a theoretical basis for the initial tsunami height distribution for the 2-D tsunami simulations. The study also works as the basis for a unified simulation method for seismic and tsunami waves (Saito & Tsushima 2016; Saito et al. 2019). However, at present, it seems that 3-D studies have not been done for meteorological tsunamis yet.

This study theoretically describes the tsunamis generated by sea-surface pressure changes in an incompressible sea. Particularly, we investigate the ocean-bottom pressure changes during the tsunami generation considering 3-D fluid motions. Besides, the formulation can include the short-wavelength tsunamis exhibiting the dispersion. Section 2 describes a 3-D theory of the tsunami generation. Section 3 visualizes and investigates the tsunami generation due to the sea-surface pressure changes based on the solutions. Considering a growing surface pressure change not moving, we simulate the tsunamis to clarify the excitation mechanism. We then simulate the tsunamis generated by a moving surface-pressure change source. We also study the role of dispersion in the meteorological tsunamis. Finally, Section 4 concludes this study.

## 2 Tsunami generation in incompressible sea

### 2.1 Fundamental equations

The Cartesian coordinate system (Fig. 1) is used for the formulation, where the $x$ and $y$ axes are in the horizontal plane and the $z$ axis is taken positive downward. The sea surface at rest is located at $z = 0$. We assume a constant sea depth located at $z = h_0$.

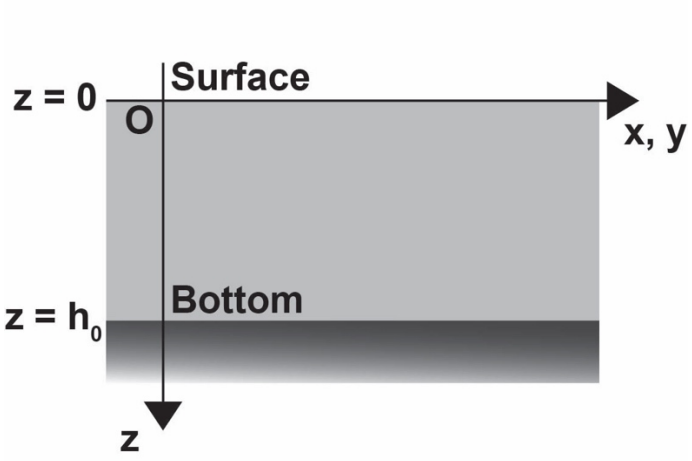


Figure 1. Coordinates used in the formulation.

Although many studies described the motion with the spatial description, or Euler description, in fluid dynamics (e.g., Pedlosky 2003), this study employs the material description, or Lagrange description (e.g., Eq. (3.57) in Dahlen & Tromp 1998; Eq. (9.26) in Segall 2010). When neglecting the change of the gravity potential due to the motion, the 3-D linear momentum equation

$$\rho_0 \frac{\partial^2 \mathbf{u}(x,y,z,t)}{\partial t^2} = \nabla \cdot \boldsymbol{\tau} + \rho_0 g_0 [\nabla u_z - (\nabla \cdot \mathbf{u}) \bar{\mathbf{e}}_z] \tag{1}$$

describes the fluid motion, where $\mathbf{u}$ is the displacement vector $\mathbf{u} = u_x \bar{\mathbf{e}}_x + u_y \bar{\mathbf{e}}_y + u_z \bar{\mathbf{e}}_z$, $\boldsymbol{\tau}$ is the stress change caused by the motion, $\rho_0$ is the density, $g_0$ is the gravitational acceleration, and $\bar{\mathbf{e}}_i$ is the basis vector for the $i$ axis. There is no shear stress in the fluid and the stress tensor is described as

$$\boldsymbol{\tau}(x,y,z,t) = -p(x,y,z,t)\mathbf{I} \tag{2}$$

where $p$ is the pressure change caused by the motion and $\mathbf{I}$ is the identity matrix. We assume an incompressible fluid:

$$\nabla \cdot \mathbf{u} = 0. \tag{3}$$

At the sea bottom, we set no vertical displacement:

$$u_z(x, y, h_0, t) = 0 \tag{4}$$

At the sea surface, we give the pressure change as

$$p(x, y, 0, t) = p_{\text{surface}}(x, y, t) \tag{5}$$

The equations of (1) – (5) describe the fluid motion. Particularly, this study considers the sea-surface pressure change Eq. (5) as the source. We will find the solutions, $\mathbf{u}(x, y, z, t)$ and $p(x, y, z, t)$. Using $u_z(x, y, z, t)$, we derive the tsunami height $\eta(x, y, t) = -u_z(x, y, 0, t)$.

## 2.2 Wavenumber integration method

To find the solutions $\mathbf{u}(x, y, z, t)$ and $p(x, y, z, t)$ that satisfy Eqs. (1) – (5), we use a wavenumber integration method. The displacements and the pressure change are represented as integrals with respect to the wavenumber and the angular frequency:

$$-p(x, y, z, t) = \frac{1}{2\pi}\int_{-\infty}^{\infty} d\omega\, e^{-i\omega t} \frac{1}{(2\pi)^2} \iint_{-\infty}^{\infty} dk_x dk_y k T_z\left(k_x, k_y, z, \omega\right) e^{i(k_x x + k_y y)} \tag{6}$$

$$u_x(x, y, z, t) = \frac{1}{2\pi}\int_{-\infty}^{\infty} d\omega\, e^{-i\omega t} \frac{1}{(2\pi)^2} \iint_{-\infty}^{\infty} dk_x dk_y \frac{ik_x}{k} U_r\left(k_x, k_y, z, \omega\right) e^{i(k_x x + k_y y)} \tag{7}$$

$$u_y(x, y, z, t) = \frac{1}{2\pi}\int_{-\infty}^{\infty} d\omega\, e^{-i\omega t} \frac{1}{(2\pi)^2} \iint_{-\infty}^{\infty} dk_x dk_y \frac{ik_y}{k} U_r\left(k_x, k_y, z, \omega\right) e^{i(k_x x + k_y y)} \tag{8}$$

$$u_z(x, y, z, t) = \frac{1}{2\pi}\int_{-\infty}^{\infty} d\omega\, e^{-i\omega t} \frac{1}{(2\pi)^2} \iint_{-\infty}^{\infty} dk_x dk_y U_z\left(k_x, k_y, z, \omega\right) e^{i(k_x x + k_y y)} \tag{9}$$

where $k = \sqrt{k_x^2 + k_y^2}$.

By substituting Eqs. (7), (8), and (9) into the condition of no dilatation (Eq. (3)), we obtain

$$-kU_r + \frac{dU_z}{dz} = 0 \tag{10}$$

From the momentum equation (Eq. (1)) with Eq. (10), we obtain the ordinal differential equations with respect to the independent variable $z$:

$$\frac{d}{dz}\begin{pmatrix} U_z \\ T_z \end{pmatrix} = \begin{pmatrix} -\dfrac{g_0 k^2}{\omega^2} & -\dfrac{k^3}{\rho_0 \omega^2} \\ -\dfrac{\rho_0 \omega^2}{k} + \dfrac{\rho_0 g_0^2 k}{\omega^2} & \dfrac{g_0 k^2}{\omega^2} \end{pmatrix} \begin{pmatrix} U_z \\ T_z \end{pmatrix}. \tag{11}$$

By evaluating the eigenvalues and eignevectors of the $2 \times 2$ matrix in Eq. (11), we can calculate the propagator matrix $\mathbf{A}(z)$ (e.g., Gilbert & Backus 1966; Aki & Richards 2002):

$$\begin{aligned} \mathbf{A}(z) &= \begin{pmatrix} A_{11}(z) & A_{12}(z) \\ A_{21}(z) & A_{22}(z) \end{pmatrix} \\ &= \begin{pmatrix} \cosh[kz] - \dfrac{g_0 k}{\omega^2}\sinh[kz] & -\dfrac{k^2}{\rho_0 \omega^2}\sinh[kz] \\ -\dfrac{\rho_0 \omega^2}{k^2}\left(1 - \dfrac{g_0^2 k^2}{\omega^4}\right)\sinh[kz] & \cosh[kz] + \dfrac{g_0 k}{\omega^2}\sinh[kz] \end{pmatrix}. \end{aligned} \tag{12}$$

This propagator matrix relates the $U_z$ and $T_z$ at different depths $z$ and $z_0$ as

$$\begin{pmatrix} U_z(k_x, k_y, z, \omega) \\ T_z(k_x, k_y, z, \omega) \end{pmatrix} = \mathbf{A}(z - z_0) \begin{pmatrix} U_z(k_x, k_y, z_0, \omega) \\ T_z(k_x, k_y, z_0, \omega) \end{pmatrix}. \tag{13}$$

The vertical displacement is zero at the sea bottom (Eq. (4)). Eq. (13) then gives the relation between the values at the surface ($z = 0$) and the bottom ($z = h_0$) as

$$\begin{aligned} \begin{pmatrix} 0 \\ T_z(k_x, k_y, h_0, \omega) \end{pmatrix} &= \mathbf{A}(h_0) \begin{pmatrix} U_z(k_x, k_y, 0, \omega) \\ T_z(k_x, k_y, 0, \omega) \end{pmatrix} \\ &= \begin{pmatrix} A_{11}(h_0) & A_{12}(h_0) \\ A_{21}(h_0) & A_{22}(h_0) \end{pmatrix} \begin{pmatrix} U_z(k_x, k_y, 0, \omega) \\ T_z(k_x, k_y, 0, \omega) \end{pmatrix}. \end{aligned} \tag{14}$$

We calculate Eq. (14) as

$$\begin{aligned} \begin{pmatrix} U_z(k_x, k_y, 0, \omega) \\ T_z(k_x, k_y, 0, \omega) \end{pmatrix} &= \begin{pmatrix} A_{11}(-h_0) & A_{12}(-h_0) \\ A_{21}(-h_0) & A_{22}(-h_0) \end{pmatrix} \begin{pmatrix} 0 \\ T_z(k_x, k_y, h_0, \omega) \end{pmatrix} \\ &= \begin{pmatrix} A_{12}(-h_0) T_z(h_0) \\ A_{22}(-h_0) T_z(h_0) \end{pmatrix}. \end{aligned} \tag{15}$$

Then, we obtain

$$T_z(k_x, k_y, h_0, \omega) = \frac{1}{A_{22}(-h_0)} T_z(k_x, k_y, 0, \omega), \tag{16}$$

and

$$\begin{aligned} U_z(k_x, k_y, 0, \omega) &= A_{12}(-h_0) T_z(k_x, k_y, h_0, \omega) \\ &= \frac{A_{12}(-h_0)}{A_{22}(-h_0)} T_z(k_x, k_y, 0, \omega). \end{aligned} \tag{17}$$

We can represent $U_z(z)$ and $T_z(z)$ using the propagator matrix as

$$U_z(k_x, k_y, z, \omega) = \frac{A_{12}(z - h_0)}{A_{22}(-h_0)} T_z(k_x, k_y, 0, \omega) \tag{18}$$

and

$$T_z(k_x, k_y, z, \omega) = \frac{A_{22}(z - h_0)}{A_{22}(-h_0)} T_z(k_x, k_y, 0, \omega). \tag{19}$$

2.3 Sudden pressure change at the sea surface

We here consider a special case in which a pressure change $p_0(x, y)$ suddenly occurs at the time $t = 0$. The surface pressure change $p_{\text{surface}}(x, y, t)$ is represented as

$$\begin{aligned} p_{\text{surface}}(x, y, t) &= p_0(x, y) H(t) \\ &= \frac{1}{2\pi} \int_{-\infty}^{\infty} d\omega \, e^{-i\omega t} \frac{1}{(2\pi)^2} \iint_{-\infty}^{\infty} dk_x dk_y \hat{p}_0(k_x, k_y) \frac{1}{-i\omega} e^{i(k_x x + k_y y)} \end{aligned} \tag{20}$$

where $H(t)$ is the step function $H(t) = 1$ when $t > +0$ and $H(t) = 0$ when $t < -0$. A comparison of Eq. (20) with Eq. (6) gives the boundary condition at the surface $T_z(k_x, k_y, 0, \omega)$ as

$$T_z(k_x, k_y, 0, \omega) = \frac{\hat{p}_0(k_x, k_y)}{k} \frac{1}{i\omega}. \tag{21}$$

With the propagator matrix (Eq.(12)) and the boundary condition (Eq. (21)), Eq. (18) is calculated as

$$\begin{aligned} U_z(k_x, k_y, z, \omega) &= \frac{A_{12}(z - h_0)}{A_{22}(-h_0)} T_z(k_x, k_y, 0, \omega) \\ &= \frac{\frac{k^2}{\rho_0 \omega^2} \sinh[k(h_0 - z)]}{\cosh[k h_0] - \frac{k g_0}{\omega^2} \sinh[k h_0]} \frac{\hat{p}_0(k_x, k_y)}{k} \frac{1}{i\omega} \\ &= \frac{\sinh[k(h_0 - z)]}{\cosh(kh)} \frac{k \hat{p}_0(k_x, k_y)}{\rho_0} \frac{1}{\omega^2 - g_0 k \tanh(k h_0)} \frac{1}{i\omega} \end{aligned} \tag{22}$$

Eqs. (22) and (10) give

$$U_r(k_x, k_y, z, \omega) = \frac{1}{k}\frac{dU_z}{dz} = -\frac{\cosh[k(h_0 - z)]}{\cosh(kh_0)}\frac{k\hat{p}_0(k_x, k_y)}{\rho_0}\frac{1}{\omega^2 - g_0 k \tanh(kh_0)}\frac{1}{i\omega} \tag{23}$$

The $T_z(k_x, k_y, z, \omega)$ is then given by

$$\begin{aligned} &T_z(k_x, k_y, z, \omega) \\ &= \frac{A_{22}(z - h_0)}{A_{22}(-h_0)} T_z(0) \\ &= \left(\frac{\omega}{i}\frac{\cosh[k(h_0 - z)]}{\cosh(kh_0)} + \frac{1}{i\omega}\frac{gk\sinh[k(h_0 - z)]}{\cosh(kh_0)}\right)\frac{1}{\omega^2 - g_0 k \tanh(kh_0)}\frac{\hat{p}_0(k_x, k_y)}{k}. \end{aligned} \tag{24}$$

Particularly, for the sea bottom ($z = h_0$), we obtain

$$\begin{aligned} T_z(k_x, k_y, h_0, \omega) &= \frac{1}{A_{22}(-h_0)} T_z(k_x, k_y, 0, \omega) \\ &= \frac{1}{\cosh(kh_0)}\frac{\hat{p}_0(k_x, k_y)}{k}\frac{\omega}{i}\frac{1}{\omega^2 - g_0 k \tanh(kh_0)}. \end{aligned} \tag{25}$$

2.4 Integration with respect to the angular frequency

With Eq. (9), the vertical displacement is represented as

$$\begin{aligned} u_z(x, y, z, t) = \frac{1}{(2\pi)^2}\iint_{-\infty}^{\infty} dk_x dk_y e^{i(k_x x + k_y y)}\frac{\sinh[k(h_0 - z)]}{\cosh(kh_0)}\frac{k\hat{p}_0(k_x, k_y)}{\rho_0} \\ \frac{1}{2\pi}\int_{-\infty}^{\infty} d\omega\, e^{-i\omega t}\frac{1}{\omega^2 - g_0 k \tanh(kh_0)}\frac{1}{i\omega} \end{aligned} \tag{26}$$

The integration with respect to the angular frequency $\omega$ is conducted with the residue theorem (**Appendix A**). Then, using the dispersion relation

$$\omega_0 = \sqrt{g_0 k \tanh(kh_0)}, \tag{27}$$

we obtain from Eq. (26)

$$
\begin{aligned}
&u_z(x,y,z,t)\\
&=\frac{1}{(2\pi)^2}\iint_{-\infty}^{\infty} dk_x dk_y e^{i(k_x x+k_y y)}\frac{k^2}{\rho_0}\frac{\sinh[k(h_0-z)]}{\cosh(kh_0)}\frac{\hat{p}_0(k_x,k_y)}{k}\frac{1}{\omega_0^2}[1\\
&\qquad -\cos(\omega_0 t)]H(t)\\
&=\frac{1}{(2\pi)^2}\iint_{-\infty}^{\infty} dk_x dk_y e^{i(k_x x+k_y y)}\frac{\hat{p}_0(k_x,k_y)}{\rho_0 g_0}\frac{\sinh[k(h_0-z)]}{\sinh(kh_0)}[1-\cos(\omega_0 t)]H(t).
\end{aligned}
\tag{28}
$$

Similarly, we obtain

$$
\begin{aligned}
&u_x(x,y,z,t)\\
&=\frac{-1}{(2\pi)^2}\iint_{-\infty}^{\infty} dk_x dk_y e^{i(k_x x+k_y y)}\frac{1}{\rho_0 g_0}\frac{ik_x}{k}\frac{\cosh[k(h_0-z)]}{\sinh(kh_0)}\hat{p}_0(k_x,k_y)[1\\
&\qquad -\cos(\omega_0 t)]H(t),
\end{aligned}
\tag{29}
$$

$$
\begin{aligned}
&u_y(x,y,z,t)\\
&=\frac{-1}{(2\pi)^2}\iint_{-\infty}^{\infty} dk_x dk_y e^{i(k_x x+k_y y)}\frac{1}{\rho_0 g_0}\frac{ik_y}{k}\frac{\cosh[k(h_0-z)]}{\sinh(kh_0)}\hat{p}_0(k_x,k_y)[1\\
&\qquad -\cos(\omega_0 t)]H(t),
\end{aligned}
\tag{30}
$$

and

$$
\begin{aligned}
&p(x,y,z,t)\\
&=\frac{1}{(2\pi)^2}\iint_{-\infty}^{\infty} dk_x dk_y e^{i(k_x x+k_y y)}p_0(k_x,k_y)\left[\frac{\cosh[k(h_0-z)]}{\cosh(kh_0)}\cos(\omega_0 t)\right.\\
&\qquad \left.+\frac{\sinh[k(h_0-z)]}{\sinh(kh_0)}(1-\cos\omega_0 t)\right]H(t)\\
&=\frac{1}{(2\pi)^2}\iint_{-\infty}^{\infty} dk_x dk_y e^{i(k_x x+k_y y)}\hat{p}_0(k_x,k_y)\left[\frac{\sinh[k(h_0-z)]}{\sinh(kh_0)}\right.\\
&\qquad \left.+\frac{2\sinh kz}{\sinh(2kh_0)}\cos\omega_0 t\right]H(t).
\end{aligned}
\tag{31}
$$

Particularly, at the sea bottom, the pressure change is given by

$$
\begin{aligned}
&p(x,y,h_0,t)\\
&=\frac{1}{(2\pi)^2}\iint_{-\infty}^{\infty} dk_x dk_y e^{i(k_x x+k_y y)}\frac{1}{\cosh(kh_0)}\hat{p}_0(k_x,k_y)\cos(\omega_0 t)\,H(t).
\end{aligned}
\tag{32}
$$

We introduce tsunami height $\eta(x,y,t)$. This is given by the vertically upward displacement at the sea surface $\eta(x,y,t)=-u_z(x,y,0,t)$:

$$\eta(x,y,t) = -u_z(x,y,0,t) = \frac{-1}{(2\pi)^2}\iint_{-\infty}^{\infty} dk_x dk_y e^{i(k_x x + k_y y)} \frac{1}{\rho_0 g_0} \hat{p}_0\left(k_x, k_y\right)[1-\cos(\omega_0 t)]H(t). \tag{33}$$

2.5 Impulse responses

Using the solutions (28) – (33), we then derive the solution with respect to the impulsive pressure change at the sea surface given by

$$p(x,y,0,t) = \delta(x,y)\delta(t). \tag{34}$$

By differentiating the solutions (28) – (33) with respect to time and replacing $\hat{p}_0\left(k_x, k_y\right)$ as $\hat{p}_0\left(k_x, k_y\right) = 1$, we calculate the wavefield solutions in the case when the surface pressure source is given by Eq. (34). For example, the vertical displacement excited by the source of Eq. (34) is calculated from Eq. (28) as

$$\bar{u}_z(x,y,z,t) = \frac{1}{(2\pi)^2}\iint_{-\infty}^{\infty} dk_x dk_y e^{i(k_x x + k_y y)} \frac{1}{\rho_0 g_0} \frac{\sinh[k(h_0 - z)]}{\sinh(kh_0)} \omega_0 \sin(\omega_0 t)\, H(t). \tag{35}$$

Here we attach a bar on the left-hand side variables as $\bar{u}_z$ rather than $u_z$ because this impulse response has a dimension that is different from $u_z$.

By differentiating Eq. (35) with respect to time, we obtain the vertical velocity as

$$\bar{v}_z(x,y,z,t) = \frac{1}{(2\pi)^2}\iint_{-\infty}^{\infty} dk_x dk_y e^{i(k_x x + k_y y)} \frac{1}{\rho_0 g_0} \frac{\sinh[k(h_0 - z)]}{\sinh(kh_0)} \omega_0^2 \cos(\omega_0 t)\, H(t). \tag{36}$$

Similarly, we obtain the horizontal velocity components:

$$\bar{v}_x(x,y,z,t) = \frac{1}{(2\pi)^2}\iint_{-\infty}^{\infty} dk_x dk_y e^{i(k_x x + k_y y)} \frac{-ik_x}{\rho_0 g_0 k} \frac{\cosh[k(h_0 - z)]}{\sinh(kh_0)} \omega_0^2 \cos(\omega_0 t)\, H(t) \tag{37}$$

and

$$\bar{v}_y(x,y,z,t) = \frac{1}{(2\pi)^2}\iint_{-\infty}^{\infty} dk_x dk_y e^{i(k_x x + k_y y)} \frac{-ik_y}{\rho_0 g_0 k} \frac{\cosh[k(h_0 - z)]}{\sinh(kh_0)} \omega_0^2 \cos(\omega_0 t)\, H(t). \tag{38}$$

The pressure change in the fluid is

$$\bar{p}(x,y,z,t) = \frac{1}{(2\pi)^2}\iint_{-\infty}^{\infty} dk_x dk_y e^{i(k_x x + k_y y)} \left[ -\frac{2\sinh(kz)}{\sinh(kh)}\omega_0 \sin(\omega_0 t)\, H(t) + \left( \frac{\sinh k(h_0 - z)}{\sinh(kh_0)} + \frac{2\sinh kz}{\sinh(2kh_0)} \right) \delta(t) \right] \tag{39}$$

In particular, for the sea bottom,

$$\bar{p}(x,y,h,t) = \frac{1}{(2\pi)^2}\iint_{-\infty}^{\infty} dk_x dk_y e^{i(k_x x + k_y y)} \frac{1}{\cosh(kh_0)} [\delta(t) - \omega_0 \sin(\omega_0 t)\, H(t)] \tag{40}$$

Eqs. (35) – (40) are the most important and fundamental solutions in our formulation, because we can obtain any responses with respect to any surface pressure change $p_{\text{surface}}(\xi_x, \xi_y, \tau)$ with convolution operations. For example, the vertical displacement response is given for an arbitrary sea-surface pressure change source $p_{\text{surface}}(\xi_x, \xi_y, \tau)$ as

$$u_z(x,y,z,t) = \iint_{-\infty}^{\infty} d\xi_x d\xi_y \int_{-\infty}^{\infty} d\tau\, \bar{u}_z\,(x - \xi_x, y - \xi_y, z, t - \tau) p_{\text{surface}}(\xi_x, \xi_y, \tau). \tag{41}$$

## 3 Visualization and Interpretations

### 3.1 Surface pressure change at a fixed location

As the simplest case, we consider the surface pressure change not to move. The pressure change starts at $t = 0$ and increases linearly with duration $T$. The sea-surface pressure source is represented as

$$p(x,y,0,t) = p_0(x,y) f(t) \tag{42}$$

where

$$p_0(x,y) = P_0 e^{-\frac{x^2}{a^2}} \tag{43}$$

and

$$f(t) = \begin{cases} \dfrac{t}{T} H(t) & \text{for } t < T \\ 1 & \text{for } T < t \end{cases}. \tag{44}$$

The 2-D Fourier transform of Eq. (43) is given by

$$\begin{aligned}\hat{p}_0(k_x,k_y) &= \iint_{-\infty}^{\infty} p_0(x,y)e^{-i(k_x x+k_y y)}dxdy \\ &= 2\pi\delta(k_y)\int_{-\infty}^{\infty} P_0 e^{-\frac{x^2}{a^2}} e^{-ik_x x}dx \\ &= 2\pi\delta(k_y)\hat{p}_1(k_x)\end{aligned} \tag{45}$$

where we set

$$\hat{p}_1(k_x) = \int_{-\infty}^{\infty} P_0 e^{-\frac{x^2}{a^2}} e^{-ik_x x}dx = \sqrt{\pi}aP_0 e^{-\frac{a^2k_x^2}{4}}. \tag{46}$$

The inverse Fourier transform with Eq. (45) gives

$$\begin{aligned}p_0(x,y) &= \frac{1}{(2\pi)^2}\iint_{-\infty}^{\infty} dk_x dk_y \hat{p}_0(k_x,k_y)\, e^{i(k_x x+k_y y)} \\ &= \frac{1}{2\pi}\int_{-\infty}^{\infty} dk_x\, \hat{p}_1(k_x)e^{ik_x x}\end{aligned} \tag{47}$$

Using the impulse responses of Eqs. (35) – (40) and the pressure change as source (42) and (47) in the convolution (see, for example, Eq. (41)), we obtain the sea-surface height change

$$\begin{aligned}&\eta(x,y,t) \\ &= -\frac{1}{2\pi}\int_{-\infty}^{\infty} dk_x e^{ik_x x}\frac{\hat{p}_1(k_x)}{\rho_0 g_0}\begin{cases}\frac{1}{\omega_0 T}[\omega_0 t - \sin(\omega_0 t)] & 0<t<T \\ \frac{1}{\omega_0 T}[\omega_0 T - \sin(\omega_0 t) + \sin[\omega_0(t-T)]] & T<t\end{cases}\end{aligned} \tag{48}$$

and the velocity fields

$$\begin{aligned}&v_z(x,y,z,t) \\ &= \frac{1}{2\pi}\int_{-\infty}^{\infty} dk_x e^{ik_x x}\frac{\sinh[|k_x|(h_0-z)]}{\sinh(|k_x|h_0)}\frac{\hat{p}_1(k_x)}{\rho_0 g_0}\begin{cases}\frac{1}{T}[1-\cos(\omega_0 t)] & 0<t<T \\ \frac{1}{T}[\cos[\omega_0(t-T)] - \cos(\omega_0 t)] & T<t\end{cases}\end{aligned} \tag{49}$$

$$\begin{aligned}&v_x(x,y,z,t) \\ &= \frac{1}{2\pi}\int_{-\infty}^{\infty} dk_x e^{ik_x x}\frac{\cosh[|k_x|(h_0-z)]}{\sinh(|k_x|h_0)}\frac{-ik_x\hat{p}_1(k_x)}{\rho_0 g_0|k_x|}\begin{cases}\frac{1}{T}[1-\cos(\omega_0 t)] & 0<t< \\ \frac{1}{T}[\cos[\omega_0(t-T)] - \cos(\omega_0 t)] & T<\end{cases}\end{aligned} \tag{50}$$

and the ocean-bottom pressure change

$$p(x, y, z = h_0, t)$$
$$= \frac{1}{2\pi}\int_{-\infty}^{\infty} dk_x e^{ik_x x} \frac{\hat{p}_1(k_x)}{\cosh(|k_x|h_0)} \begin{cases} \frac{1}{\omega_0 T}\sin(\omega_0 t) & 0 < t < T \\ \frac{1}{\omega_0 T}[\sin(\omega_0 t) - \sin[\omega_0(t-T)]] & T < t \end{cases} \quad (51)$$

Using these solutions with the depth $h_0 = 4$ km and setting $P_0 = -1$ mH$_2$O (~9.8 kPa), $a = 20$ km, and $T = 30$ s as a source (Eq. (42)), we numerically calculate and visualize the tsunami generation and propagation for negative sea-surface pressure change in Fig. 2.

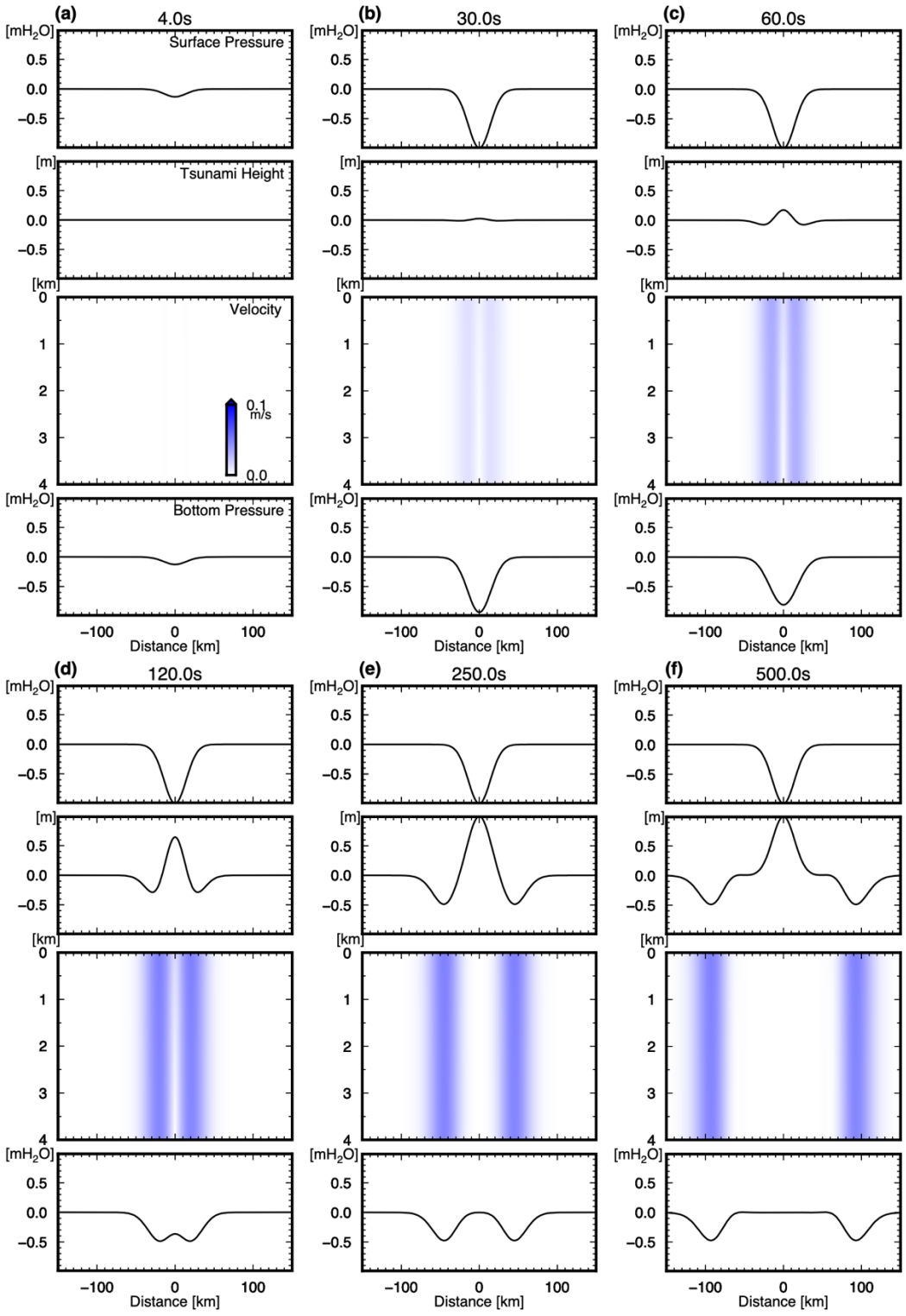


Figure 2. Tsunami generation due to a non-moving surface pressure change for various elapsed times: (a) $t = 4$, (b) 30, (c) 60, (d) 120, (e) 250, and (f) 500s. Top panels show the pressure change at the surface where the peak pressure change is $P_0 = -1$ mH$_2$O ($\sim -9.8$ kPa), the duration is $T = 30$ s and the spatial scale is

given by $a = 20$ km in Eqs. (42) and (43). Second panels show tsunami height or vertical upward displacement at the sea surface. Third panels show velocity distribution $\sqrt{v_x^2 + v_z^2}$ in the sea layer with the depth $h_0$ = 4 km. Bottom panels show the pressure change at the sea bottom.

Figs 2a and 2b show that the sea-surface pressure, which we set as a source, decreases with the time until $t = T$ (= 30 s). During this period, the sea-surface height and the velocity in the sea layer change slightly and do not show significant variations (the second and third panels in Figs 2a and 2b). As the time elapses (60 – 120s, Figs 2c-2d), the sea-surface height gradually increases. At the time of 250 s (Fig. 2e), the sea-surface uplift reached 1.0 m. While the sea-surface height is uplifted inside the pressure source, the surface height is subsided outside the pressure source ($x$ <~–30 km and $x$ >~30 km in the second panels in Figs 2d and 2e) so as to satisfy the water volume conservation. The water volume is displaced horizontally. The displacement propagates as tsunamis.

We should note that the source duration of $T$= 30 s we set in this simulation is shorter than a characteristic time given by $2a/c$ =200 s. This characteristic time is a time scale for a tsunami propagating the distance of the source size or the time for the initial tsunami height to collapse, roughly corresponding to the time the sea-surface height inside the source reaches equilibrium (Fig. 2e). If we set the duration $T$ longer than the characteristic time $2a/c$, the amplitude of the leading tsunamis become smaller (e.g., Saito & Furumura 2009).

The bottom pressure change (the bottom panels in Fig. 2) increases with the time in Figs 2c – 2e. The increasing sea-surface height makes the pressure change at the sea bottom less. As more time elapses (Fig. 2f), the sea surface remains uplifted (top second panel in Fig. 2f) to compensate the surface-pressure source, and the horizontally displaced water volume propagates as a tsunami ($x$ <~–30 km and $x$ >~30 km in top second panel in Fig. 2f). The propagating tsunamis are detectable as ocean-bottom pressure changes.

### 3.2 A comparison with the tsunamis generated by an earthquake

The surface pressure change $p(x, y, 0, t) = p_0(x, y)H(t)$ generates tsunamis that are identical to the tsunamis generated by the initial height distribution $\eta(x, y, t = 0)$ given by

$$\eta(x, y, t = 0) = \frac{p_0(x, y)}{\rho_0 g_0}. \tag{52}$$

In other words, here, $\eta(x, y, 0)$ is the equivalent initial tsunami height for the pressure change source $p_0(x, y)H(t)$. The 3-D formulation in this study derives this equivalence between the sea-surface pressure change source and the initial height distribution source only for the tsunamis outside the source region. From Eq. (33), we represent the tsunamis caused by the surface pressure change as two terms:

$$\begin{aligned}&\eta(x,y,t)\\&=\frac{-1}{(2\pi)^2}\iint_{-\infty}^{\infty}dk_xdk_ye^{i(k_xx+k_yy)}\frac{1}{\rho_0g_0}p_0\big(k_x,k_y\big)H(t)\\&\qquad+\frac{1}{(2\pi)^2}\iint_{-\infty}^{\infty}dk_xdk_ye^{i(k_xx+k_yy)}\frac{1}{\rho_0g_0}p_0\big(k_x,k_y\big)\cos(\omega_0t)\,H(t).\end{aligned}\tag{53}$$

Note that the first term contributes to only inside the surface pressure change but does not contribute to outside the surface pressure change (i.e., the area where $p_0(x,y)=0$) since it does not propagate. On the other hand, the second term contributes to the tsunamis outside the pressure change since it does propagate as waves due to the factor of $\cos(\omega_0t)$. As a result, the tsunami outside the source region is given by

$$\eta_{outside}^{surface}(x,y,t)=\frac{1}{(2\pi)^2}\iint_{-\infty}^{\infty}dk_xdk_ye^{i(k_xx+k_yy)}\frac{1}{\rho_0g_0}p_0\big(k_x,k_y\big)\cos(\omega_0t)\,H(t)\tag{54}$$

For the tsunamis caused by the sea-bottom deformation (see Appendix B), the tsunami height $\eta^{bottom}(x,y,t)$ is given by

$$\begin{aligned}\eta^{bottom}(x,y,t)&=\frac{-1}{(2\pi)^2}\iint_{-\infty}^{\infty}dk_xdk_ye^{i(k_xx+k_yy)}\frac{\hat{u}_0\big(k_x,k_y\big)}{\cosh kh_0}\cos(\omega_0t)\,H(t)\\&=\frac{1}{(2\pi)^2}\iint_{-\infty}^{\infty}dk_xdk_ye^{i(k_xx+k_yy)}\hat{\eta}_0\big(k_x,k_y\big)\cos(\omega_0t)\,H(t)\end{aligned}\tag{55}$$

where $\hat{u}_0\big(k_x,k_y\big)$ and $\hat{\eta}_0\big(k_x,k_y\big)$ are the 2-D spatial Fourier transform of the sea-bottom vertical displacement $u_0(x,y)$ and the corresponding initial tsunami height distribution $\eta_0(x,y)$, respectively. Using Eqs. (54) and (55), we confirmed that $\eta_{outside}^{surface}(x,y,t)=\eta^{bottom}(x,y,t)$ if we set

$$\hat{\eta}_0\big(k_x,k_y\big)=-\frac{\hat{u}_0\big(k_x,k_y\big)}{\cosh kh_0}=\frac{\hat{p}_0\big(k_x,k_y\big)}{\rho_0g_0}\ \text{or}\ \eta_0(x,y)=\frac{p_0(x,y)}{\rho_0g_0}.\tag{56}$$

However, we should note that this situation differs for the wavefields inside the source regions. For example, the pressure change at the sea bottom caused by the sea-bottom vertical displacement distribution $u_0(x,y)$ is given by Eq. (B14) in Appendix B as

$$\begin{aligned}&p^{bottom}(x,y,h_0,t)\\&=\frac{1}{(2\pi)^2}\iint_{-\infty}^{\infty}dk_xdk_ye^{i(k_xx+k_yy)}\left[-\frac{\rho_0g_0\hat{u}_0\big(k_x,k_y\big)}{[\cosh(kh_0)]^2}\cos(\omega_0t)\,H(t)\right.\\&\qquad\left.-\rho_0h\frac{\tanh(kh_0)}{kh_0}\hat{u}_0\big(k_x,k_y\big)\delta'(t)\right]+\rho_0g_0u_0(x,y)H(t).\end{aligned}\tag{57}$$

On the other hand, the pressure change by the corresponding surface-pressure change source is given by Eqs. (32) and (56) as

$$
\begin{aligned}
p(x,y,h,t) &= \frac{1}{(2\pi)^2}\iint_{-\infty}^{\infty} dk_x dk_y e^{i(k_x x+k_y y)} \frac{1}{\cosh(kh_0)} \hat{p}_0\left(k_x,k_y\right)\cos(\omega_0 t)\,H(t) \\
&= -\frac{1}{(2\pi)^2}\iint_{-\infty}^{\infty} dk_x dk_y e^{i(k_x x+k_y y)} \frac{\rho_0 g_0 \hat{u}_0\left(k_x,k_y\right)}{[\cosh(kh_0)]^2}\cos(\omega_0 t)\,H(t)
\end{aligned}
\tag{58}
$$

We find that that the two pressure changes do not agree, $p(x,y,h_0,t) \neq p^{bottom}(x,y,h_0,t)$ inside the pressure change source. Such disagreement is also found in the tsunami height and velocity fields inside the pressure change source. These disagreements were not detectable for the past observations in which tsunami sensors were located only outside the source region. However, this difference should appear in recent tsunami observations which are intended to detect tsunamis inside the source region.

### 3.3 Moving surface pressure change

We suppose a moving pressure change with the propagation velocity $V_0$ in the *x* direction given by

$$
\begin{aligned}
p_{\text{surface}}(x,y,t) &= p_1(x-V_0 t)H(t) \\
&= P_0 e^{-\frac{(x-V_0 t)^2}{a^2}} H(t)
\end{aligned}
\tag{59}
$$

The vertical upward displacement, the velocities inside the sea layer, and the pressure change at the sea bottom are obtained by the convolution of the pressure change (59) with the impulse responses of Eqs. (35) – (40). The vertical upward displacement is

$$
\begin{aligned}
&\eta(x,y,t) \\
&= -u_z(x,y,0,t) \\
&= -\iint_{-\infty}^{\infty} d\xi_x d\xi_y \int_{-\infty}^{\infty} d\tau\, \bar{u}_z\left(x-\xi_x, y-\xi_y, 0, t-\tau\right) p_{\text{surface}}\left(\xi_x,\xi_y,\tau\right) \\
&= -\frac{1}{2\pi}\int_{-\infty}^{\infty} dk_x e^{ik_x x}\frac{\hat{p}_1(k_x)}{\rho_0 g_0}\left[\frac{1}{1-\frac{k_x^2 V_0^2}{\omega_0^2}} e^{-ik_x V t} - \frac{1}{2}\frac{1}{1-\frac{k_x V_0}{\omega_0}} e^{-i\omega_0 t}\right. \\
&\qquad\qquad \left. -\frac{1}{2}\frac{1}{1+\frac{k_x V_0}{\omega_0}} e^{i\omega_0 t}\right] H(t)
\end{aligned}
\tag{60}
$$

where $\hat{p}_1(k_x)$ is the 1-D spatial Fourier transform of $p_0(x)$. Eq. (60) corresponds to Eq. (2.4) in Proudman (1929) but is not the same because we give the 3-D case including the dispersion, while 2-D without the dispersion was derived in Proudman (1929). Using $k = |k_x|$, the horizontal and the vertical velocities are given by

$$
\begin{aligned}
&v_x(x,y,z,t)\\
&=\frac{1}{2\pi}\int_{-\infty}^{\infty}dk_x\, e^{ik_x x}\frac{\hat{p}_1(k_x)}{\rho_0 g_0}\frac{\cosh[k(h_0-z)]}{\sinh(kh_0)}\omega_0\left[-\frac{kV}{\omega_0}\frac{1}{1-\frac{k^2V_0^2}{\omega_0^2}}e^{-ik_xV_0t}\right.\\
&\qquad\left.+\frac{k_x}{2k}\frac{1}{1-\frac{k_xV_0}{\omega_0}}e^{-i\omega_0t}-\frac{k_x}{2k}\frac{1}{1+\frac{k_xV_0}{\omega_0}}e^{i\omega_0t}\right]H(t)
\end{aligned}
\tag{61}
$$

and

$$
\begin{aligned}
&v_z(x,y,z,t)\\
&=\frac{1}{2\pi}\int_{-\infty}^{\infty}dk_x\, e^{ik_x x}\frac{\hat{p}_1(k_x)}{\rho_0 g_0}\frac{\sinh[k(h_0-z)]}{\sinh(kh_0)}i\omega_0\left[\frac{-\frac{k_xV_0}{\omega_0}}{1-\frac{k^2V_0^2}{\omega_0^2}}e^{-ik_xV_0t}\right.\\
&\qquad\left.+\frac{1}{2}\frac{1}{1-\frac{k_xV_0}{\omega_0}}e^{-i\omega_0t}-\frac{1}{2}\frac{1}{1+\frac{k_xV_0}{\omega_0}}e^{i\omega_0t}\right]H(t).
\end{aligned}
\tag{62}
$$

The pressure change is given by

$$
\begin{aligned}
&p(x,y,z,t)\\
&=-\frac{1}{2\pi}\int_{-\infty}^{\infty}dk_x e^{ik_x x}\,\hat{p}_1(k_x)\frac{2\sinh(kz)}{\sinh(2kh_0)}\left[\frac{1}{1-\frac{k^2V_0^2}{\omega_0^2}}e^{-ik_xV_0t}-\frac{1}{2}\frac{1}{1-\frac{k_xV_0}{\omega_0}}e^{-i\omega_0t}\right.\\
&\qquad\left.-\frac{1}{2}\frac{1}{1+\frac{k_xV_0}{\omega_0}}e^{i\omega_0t}\right]H(t)\\
&+\frac{1}{2\pi}\int_{-\infty}^{\infty}dk_x e^{ik_x(x-V_0t)}\hat{p}_1(k_x)\left[\frac{\sinh[k(h_0-z)]}{\sinh(kh_0)}+\frac{2\sinh(kz)}{\sinh(2kh_0)}\right]H(t).
\end{aligned}
\tag{63}
$$

and

$$
\begin{aligned}
&p(x, y, z = h_0, t) \\
&= -\frac{1}{2\pi}\int_{-\infty}^{\infty} dk_x e^{ik_x x}\frac{\hat{p}_1(k_x)}{\cosh(kh_0)}\left[\frac{1}{1-\frac{k^2V_0^2}{\omega_0^2}}e^{-ik_xV_0t} - \frac{1}{2}\frac{1}{1-\frac{k_xV_0}{\omega_0}}e^{-i\omega_0 t}\right. \\
&\qquad\left. - \frac{1}{2}\frac{1}{1+\frac{k_xV_0}{\omega_0}}e^{i\omega_0 t}\right]H(t) \\
&\quad + \frac{1}{2\pi}\int_{-\infty}^{\infty} dk_x e^{ik_x(x-V_0t)}\frac{\hat{p}_1(k_x)}{\cosh(kh_0)}H(t).
\end{aligned}
\tag{64}
$$

3.3.1 Long-wavelength tsuanmis

Using Eqs. (60) – (64), we visualize the wavefields caused by a moving negative pressure change in Fig. 3. The pressure change source is characterized by $P_0 = -1$ mH$_2$O (=$\sim -9.8$ kPa) and $a = 20$km in Eq. (59). The pressure change source appears at $t = 0$ s and moves in the positive $x$ direction with the velocity $V_0 = 0.18$ km/s ($= 0.9\sqrt{g_0 h}$). At early times (Figs 3a and 3b), the tsunami height is small, less than 0.1 m. As the time increases, the tsunami height increases. At the time 500 s, the maximum height is about 2.5 m, which is considerably larger than the maximum height of 1 m that was observed in the case of a fixed source. This tsunami amplification is due to a moving source, which is often referred to as the Proudman effect (Proudman 1929).

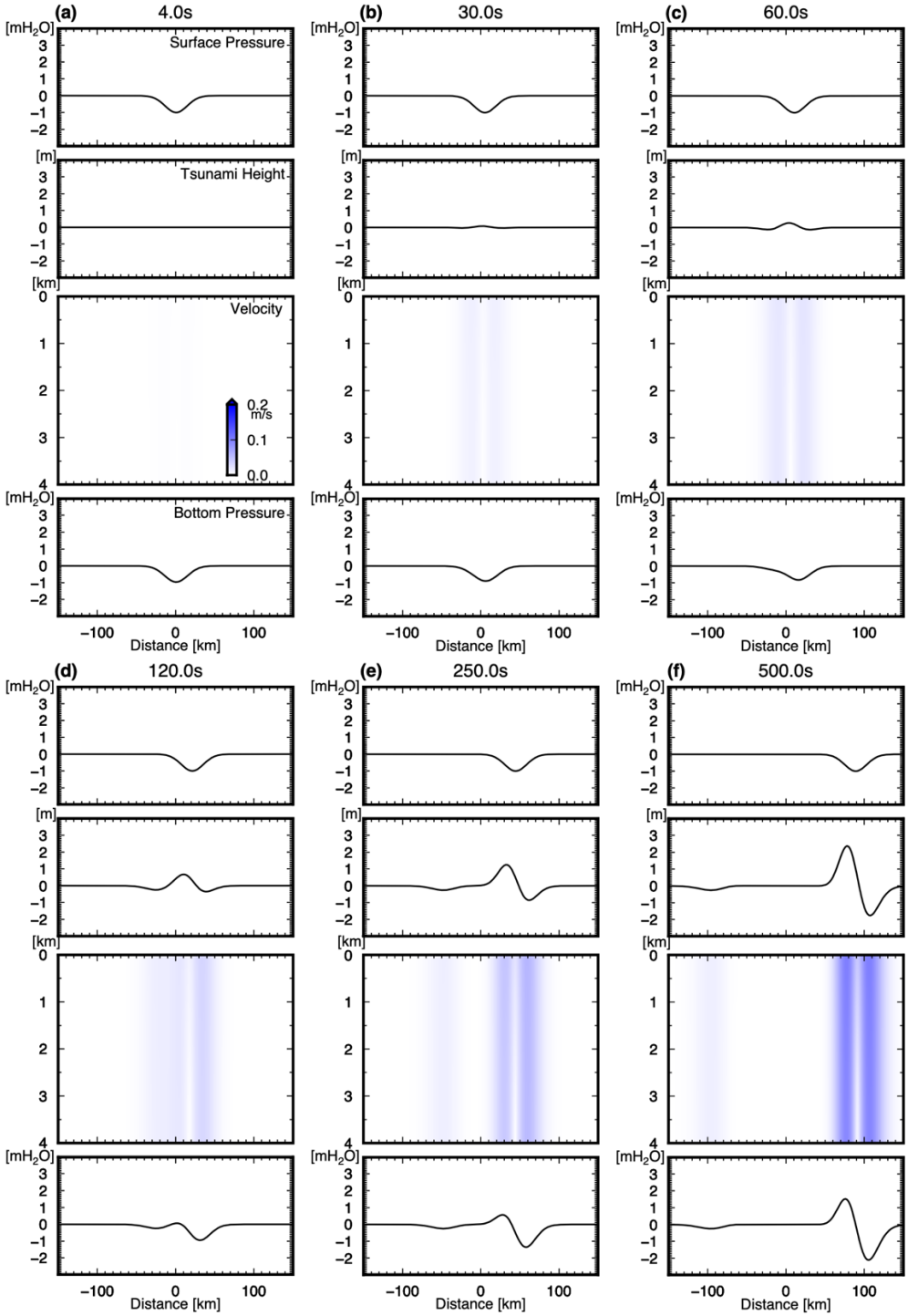


Figure 3. Tsunami generation due to a moving surface pressure change for various elapsed times: (a) $t = 4$, (b) 30, (c) 60, (d) 120, (e) 250, and (f) 500s. Top panel shows the pressure change at the surface. The source is given by Eq. (59) where the peak pressure change is $P_0 = -1$ mH₂O ($\sim -9.8$ kPa), the duration is $T = 30$ s, the spatial scale is given by $a = 20$ km, and the velocity is given by $V_0 = 0.18$ km/s ($= 0.9\sqrt{g_0 h_0}$ and $h_0 = 4$ km). Second panels show tsunami height or vertical upward displacement at the sea surface. Third panels show velocity

distribution $\sqrt{v_x^2 + v_z^2}$ in the sea layer with the depth $h_0$ = 4 km. Bottom panels show the pressure change at the sea bottom.

We further calculate the sea-surface height of Eq.(60) using approximations to obtain interpretations of Fig. 3. Since $p_1(x)$ is real, $\hat{p}_1(-k_x) = \hat{p}_1^*(k_x)$ where the asterisk denotes complex conjugation. We calculate Eq. (60):

$$\begin{aligned}\eta(x,y,t) &= -\frac{1}{\pi}\int_0^\infty dk_x \frac{1}{\rho_0 g_0}\left[\frac{1}{1-\frac{k_x^2 V_0^2}{\omega_0^2}}\mathrm{Re}\left[\hat{p}_1(k_x)e^{ik_x(x-V_0t)}\right]\right. \\ &\quad -\frac{1}{2}\frac{1}{1-\frac{k_x V_0}{\omega_0}}\mathrm{Re}\left[\hat{p}_1(k_x)e^{i(k_x x-\omega_0 t)}\right] \\ &\quad \left.-\frac{1}{2}\frac{1}{1+\frac{k_x V_0}{\omega_0}}\mathrm{Re}\left[\hat{p}_1(k_x)e^{i(k_x x+\omega_0 t)}\right]\right]H(t)\end{aligned} \tag{65}$$

where Re $[\cdots]$ indicates the real part of the complex value. We here assume that the pressure change propagation velocity $V_0$ is almost the same as the tsunami phase velocity $c$, or $V_0 \sim c$, where we set the phase velocity as $c = \omega/|k_x| = \omega/k$. Setting $c = V_0 + \Delta V$ and $\Delta V \ll V_0$, we calculate Eq. (65):

$$
\begin{aligned}
&\eta(x,y,t)\\
&= -\frac{1}{\pi}\int_0^\infty dk_x \frac{1}{\rho_0 g_0}\frac{1}{1-\frac{V_0}{c}}\left[\frac{1}{1+\frac{V_0}{c}}\mathrm{Re}\left[\hat{p}_1(k_x)e^{ik_x(x-V_0t)}\right]\right.\\
&\qquad\left.-\frac{1}{2}\mathrm{Re}\left[\hat{p}_1(k_x)e^{ik_x(x-ct)}\right]\right]H(t)\\
&\qquad+\frac{1}{\pi}\int_0^\infty dk_x \frac{1}{2}\frac{1}{\rho_0 g_0}\frac{1}{1+\frac{V_0}{c}}\mathrm{Re}\left[\hat{p}_1(k_x)e^{ik_x(x+ct)}\right]H(t)\\
&= -\frac{1}{\pi}\int_0^\infty dk_x \frac{1}{\rho_0 g_0}\frac{c}{\Delta V}\left[\frac{1}{2}\left(1-\frac{1}{2}\frac{\Delta V}{c}\right)^{-1}\mathrm{Re}\left[\hat{p}_1(k_x)e^{ik_x(x-V_0t)}\right]\right.\\
&\qquad\left.-\frac{1}{2}\mathrm{Re}\left[\hat{p}_1(k_x)e^{ik_x(x-V_0t)}e^{-ik_x\Delta Vt}\right]\right]H(t)\\
&\qquad+\frac{1}{\pi}\int_0^\infty dk_x \frac{1}{2}\frac{1}{\rho_0 g_0}\frac{1}{2}\left(1-\frac{1}{2}\frac{\Delta V}{c}\right)^{-1}\mathrm{Re}\left[\hat{p}_1(k_x)e^{ik_x(x+ct)}\right]H(t)\\
&\approx -\frac{1}{\pi}\int_0^\infty dk_x \frac{1}{\rho_0 g_0}\frac{c}{\Delta V}\mathrm{Re}\left[\frac{1}{2}\hat{p}_1(k_x)e^{ik_x(x-V_0t)}\left(1-e^{-ik_x\Delta Vt}\right)\right.\\
&\qquad\left.+\frac{1}{4}\frac{\Delta V}{c}\hat{p}_1(k_x)e^{ik_x(x-V_0t)}\right]H(t)\\
&\qquad+\frac{1}{\pi}\int_0^\infty dk_x \frac{1}{2}\frac{1}{\rho_0 g_0}\frac{1}{2}\left(1+\frac{1}{2}\frac{\Delta V}{c}\right)\mathrm{Re}\left[\hat{p}_1(k_x)e^{ik_x(x+ct)}\right]H(t)\\
&\approx -\frac{1}{\pi}\int_0^\infty dk_x \frac{1}{2\rho_0 g_0}ct\mathrm{Re}\left[ik_x\hat{p}_1(k_x)e^{ik_x(x-V_0t)}\right]H(t)\\
&\qquad-\frac{1}{\pi}\int_0^\infty dk_x \frac{1}{4\rho_0 g_0}Re\left[\hat{p}_1(k_x)e^{ik_x(x-V_0t)}\right]H(t)\\
&\qquad+\frac{1}{\pi}\int_0^\infty dk_x \frac{1}{4\rho_0 g_0}\mathrm{Re}\left[\hat{p}_1(k_x)e^{ik_x(x+ct)}\right]H(t).
\end{aligned}
\tag{66}
$$

In particular, when the wavelength is much longer than the sea depth, $kh_0 \ll 1$, the phase velocity $c$ is independent of the wavenumber. Also, using the relation

$$
\begin{aligned}
p_1(x) &= \frac{1}{2\pi}\int_{-\infty}^{\infty} dk_x\, e^{ik_x x}\hat{p}_1(k_x)\\
&= \frac{1}{\pi}\int_0^\infty dk_x\, \mathrm{Re}\left[e^{ik_x x}\hat{p}_1(k_x)\right]
\end{aligned}
\tag{67}
$$

we obtain

$$\eta(x,y,t) \approx -\frac{1}{2\rho_0 g_0} ct \frac{d}{dx} p_1(x - V_0 t)H(t) - \frac{1}{4\rho_0 g_0} p_1(x - V_0 t)H(t) + \frac{1}{4\rho_0 g_0} p_1(x + ct)H(t) \tag{68}$$

The first and the second terms indicate the waves propagating along the positive $x$ direction. In particular, the first term increases with increasing the time or increases with the travel distance $ct$. As a result, the first term becomes dominant over the second term for long travel distance. The waveform is given by the spatial derivative of the pressure change distribution. This feature is confirmed in Fig. 3.

Similarly, the pressure change at the sea bottom (Eq. (64)) is calculated as

$$\begin{aligned}
&p(x,y,z=h_0,t) \\
&= -\frac{1}{\pi}\int_0^\infty dk_x \frac{1}{\cosh(kh_0)} \Bigg[ \frac{1}{1 - \frac{k^2 V_0^2}{\omega_0^2}} \mathrm{Re}\left[\hat{p}_1(k_x) e^{ik_x(x - V_0 t)}\right] \\
&\qquad - \frac{1}{2} \frac{1}{1 - \frac{k_x V_0}{\omega_0}} \mathrm{Re}\left[\hat{p}_1(k_x) e^{i(k_x x - \omega_0 t)}\right] \\
&\qquad - \frac{1}{2} \frac{1}{1 + \frac{k_x V_0}{\omega_0}} \mathrm{Re}\left[\hat{p}_1(k_x) e^{i(k_x x + \omega_0 t)}\right] \Bigg] H(t) \\
&\qquad + \frac{1}{\pi}\int_0^\infty dk_x \frac{1}{\cosh(kh_0)} \mathrm{Re}\left[\hat{p}_1(k_x) e^{ik_x(x - V_0 t)}\right] H(t) \\
&\approx -\frac{1}{\pi}\int_0^\infty dk_x \frac{1}{2\cosh(kh_0)} ct \mathrm{Re}\left[ik_x \hat{p}_1(k_x) e^{ik_x(x - V_0 t)}\right] H(t) \\
&\qquad - \frac{1}{\pi}\int_0^\infty dk_x \frac{1}{4\cosh(kh_0)} \mathrm{Re}\left[\hat{p}_1(k_x) e^{ik_x(x - V_0 t)}\right] H(t) \\
&\qquad + \frac{1}{\pi}\int_0^\infty dk_x \frac{1}{4\cosh(kh_0)} \mathrm{Re}\left[\hat{p}_1(k_x) e^{ik_x(x + ct)}\right] H(t) \\
&\qquad + \frac{1}{\pi}\int_0^\infty dk_x \frac{1}{\cosh(kh_0)} \mathrm{Re}\left[\hat{p}_1(k_x) e^{ik_x(x - V_0 t)}\right] H(t).
\end{aligned} \tag{69}$$

For the long-wavelength tsunamis $kh_0 \ll 1$, we obtain

$$
\begin{aligned}
p(x,y,h,t) &\approx -\frac{1}{2}ct\frac{d}{dx}p_1(x-V_0t)H(t)+\frac{3}{4}p_1(x-V_0t)H(t) \\
&\quad +\frac{1}{4}p_1(x+ct)H(t) \\
&= \rho_0 g_0 \eta(x,y,t)+p_{\mathrm{surface}}(x,y,t).
\end{aligned}
\tag{70}
$$

The pressure change is given by the sum of two contributions: sea-surface height change $\rho_0 g_0 \eta(x,y,t)$ and pressure change loaded at the sea surface $p_{\mathrm{surface}}(x,y,t)$. This indicates that it is not straightforward to measure the tsunami height $\eta(x,y,t)$ correctly from the ocean-bottom pressure change $p(x,y,h_0,t)$. We need to know the sea-surface pressure change $p_{\mathrm{surface}}(x,y,t)$ to correctly estimate $\eta(x,y,t)$. For example, for the case of the time 60 s (Fig. 3c), the ocean-bottom pressure change is negative $-0.5$ $\mathrm{mH_2O}$. However, the actual tsunami height is positive (0.5 m).

### 3.3.2 Short-wavelength tsunamis

We next simulate the case of a shorter wavelength ($a = 10$ km in Eq. (59)) pressure change source, where the wavelength of the pressure change is not much longer than the sea depth. Fig. 4 shows the wavefields for various elapsed times. In Fig. 5, in order to compare dispersive and non-dispersive tsunamis, we also plot the wavefields without dispersion by setting $\omega_0 = k\sqrt{g_0 h_0}$ in Eqs. (60)-(64) instead of setting the dispersion relation of Eq. (26). Comparing Fig. 4 with Fig. 5, we recognized that the maximum tsunami increased more with increasing the time or the travel distance due to the wave dispersion. Fig. 6 shows the maximum sea-surface height for different travel distances. The maximum height gets much higher than the case without the wave dispersion. It is interesting that the dispersion can enlarge the short-wavelength tsunami height for this moving pressure change source, although the dispersion often reduces the maximum sea-surface height of tsunamis arising from, for example, thrust fault earthquakes (e.g., Saito et al. 2014). A dispersive-tsunami amplification was also found in landslide tsunamis dominated by short-wavelength waves (Baba et al. 2019).

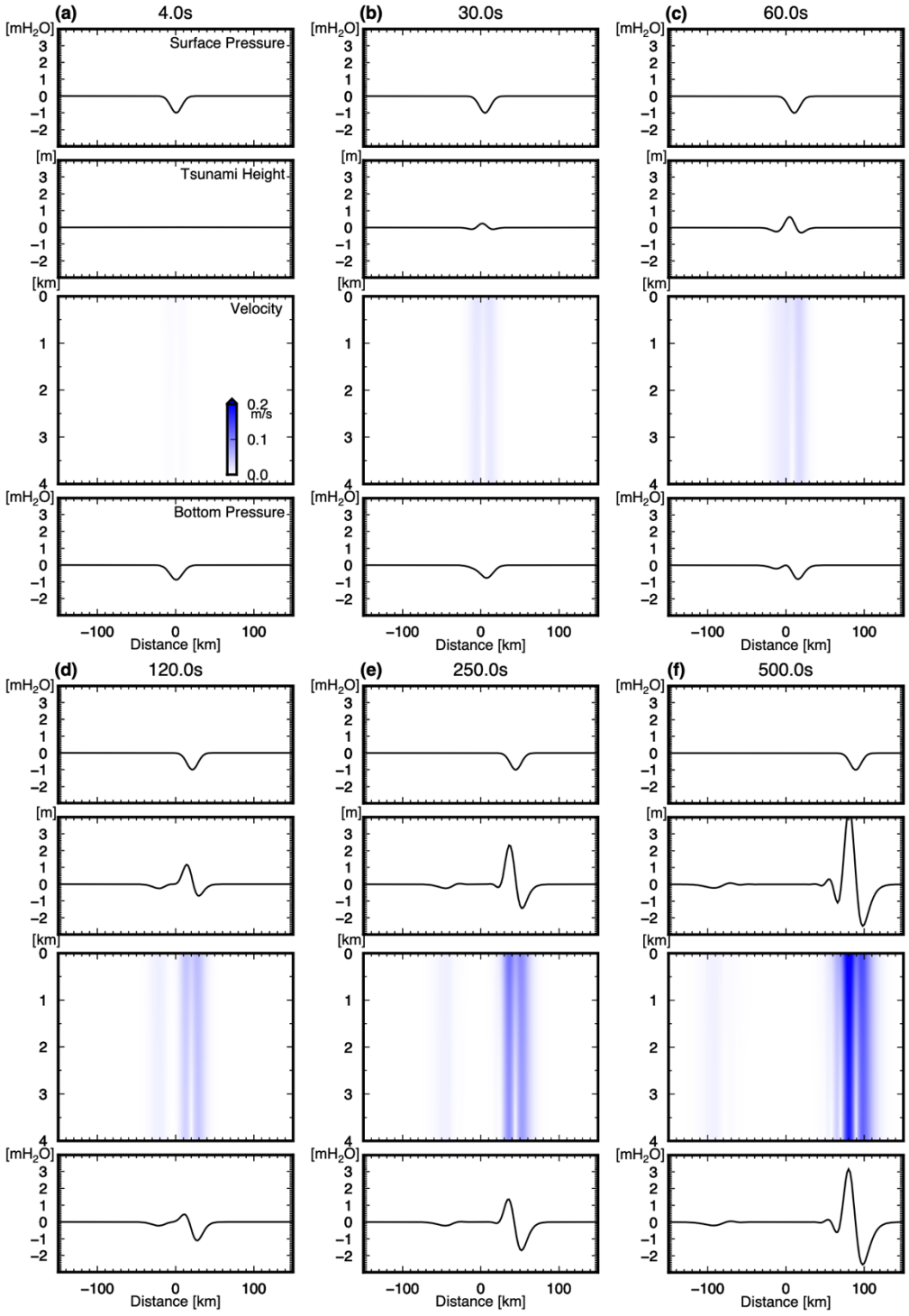


Figure 4. Tsunami generation due to a moving surface pressure change for various elapsed times: (a) $t = 4$, (b) 30, (c) 60, (d) 120, (e) 250, and (f) 500s. Top panel shows the pressure change at the surface. The source is given by Eq. (59) where the peak pressure change is $P_0 = -1$ mH$_2$O ($\sim -9.8$ kPa), the duration is $T = 30$ s, the spatial scale is given by $a = 10$ km, and the velocity is given by $V_0 = 0.18$ km/s ($= 0.9\sqrt{g_0 h_0}$ and $h_0 = 4$ km). Second panels show tsunami height or

vertical upward displacement at the sea surface. Third panels show velocity distribution $\sqrt{v_x^2 + v_z^2}$ in the sea layer with the depth $h_0$ = 4 km. Bottom panels show the pressure change at the sea bottom.

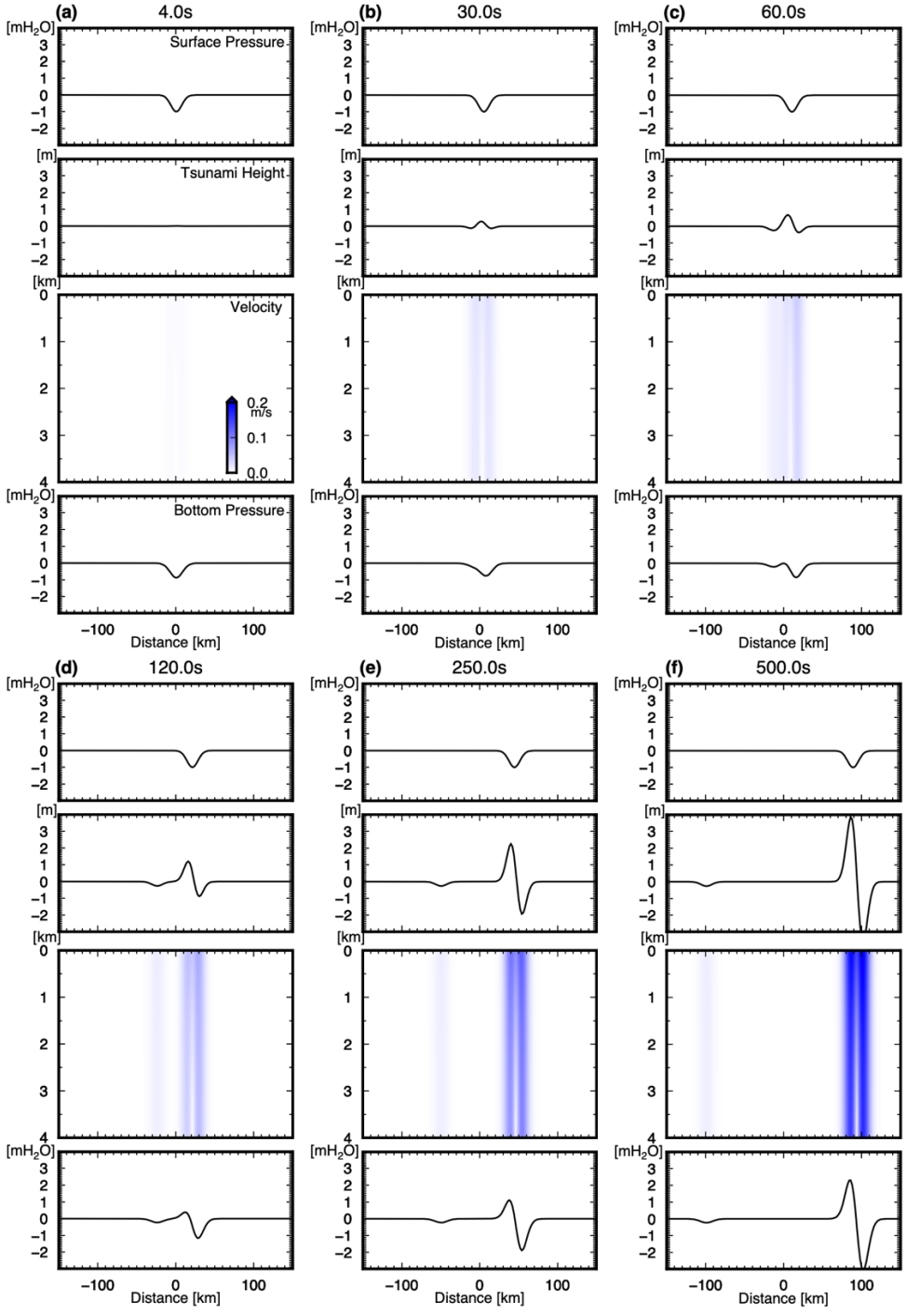


Figure 5. Tsunami generation due to a moving surface pressure change. Instead of the dispersion relation $\omega_0 = \sqrt{g_0 k \tanh(kh_0)}$ (Eq. (27)), we set $\omega_0 = k\sqrt{g_0 h_0}$ in

this simulation to remove wave dispersion. Other parameters are the same as those in Fig. 4.

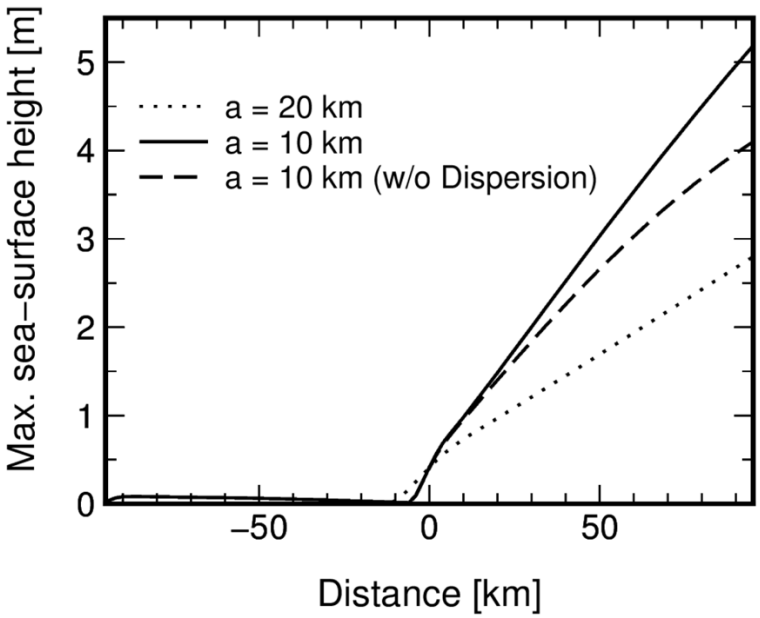


Figure 6 Maximum sea-surface height distributions for various moving source cases. The dotted line represents the case when the pressure change source is characterized by $a = 20$ km in Fig. 3. The solid line represents the case when the pressure change source is characterized by $a = 10$ km in Fig. 4. The dashed line represents the case when the pressure change source is characterized by $a = 10$ km but $\omega_0 = k\sqrt{g_0 h_0}$ to exclude the dispersion in Fig. 5.

## 4 Conclusions

We formulated 3-D tsunami generation by pressure changes on the sea surface in an incompressible sea. Using 3-D solutions, we can describe the depth-dependent generation field. As a simple case, we simulated the tsunami generation by a growing pressure change at a fixed location. We found that a negative sea-surface pressure change made the sea-surface height uplifted inside the source region and negative leading waves radiated from the source. We also simulated a case when the tsunamis are generated by a moving pressure change. When the pressure change migrates near the tsunami-propagation velocity, tsunami height increases with increasing travel distance. This was originally predicted by Proudman (1929) in the 2-D long-wave theory. The solutions in this study are in the 3-D space that can include the depth-dependent particle velocities and pressure distributions in the sea. The derived solutions of the pressure changes suggest that both the tsunami height and the sea-surface pressure changes contribute to the ocean-bottom pressure change. This means that we can detect tsunamis by ocean-bottom pressure gauges but need to know the sea-surface pressure change to correctly

measure tsunami height by the pressure gauges. Moreover, when the pressure change source was characterized by short-wavelength components, tsunamis showed the dispersion. The dispersion possibly increases tsunami height more extensively than the predictions assuming non-dispersive tsunamis. The solutions derived in this study are useful for recent offshore tsunami observations where the pressure gauges possibly detect the tsunami generation process with meteorological origins.

**Appendix A: Integration using residue theorem**

The vertical displacement $u_z(x, y, z, t)$ (Eq. (26)) includes an integration with respect to $\omega$:

$$f(t) = \frac{1}{2\pi}\int_{-\infty}^{\infty} d\omega\, e^{-i\omega t}\frac{1}{\omega^2 - \omega_0^2}\frac{1}{i\omega} \tag{A1}$$

where

$$\omega_0 = \sqrt{g_0 k \tanh(kh_0)} \tag{A2}$$

Here, we introduce an artificial damping into (A1) using very small parameters $\epsilon_1$ and $\epsilon_2$ and consider a closed complex integral on the complex $\omega$ plane

$$g(t) = \frac{1}{2\pi}\oint d\omega\, e^{-i\omega t}\frac{1}{\omega^2 + i2\epsilon_1\omega - \omega_0^2}\frac{1}{i(\omega + i\epsilon_2)} \tag{A3}$$

Fig. A1 shows the complex $\omega$ plane for Eq. (A3), where the poles are located at

$$\omega = \omega_0 - i\epsilon_1, -\omega_0 - i\epsilon_1, -i\epsilon_2. \tag{A4}$$

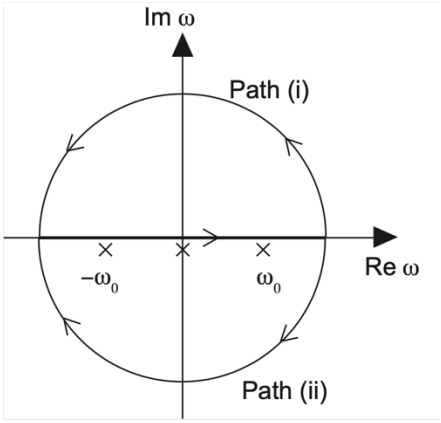


Figure A1 Integration paths of the complex integration for Eq. (A3)

For $t < 0$, we take the closed integration path (i) in the region Im $\omega > 0$. There are no poles inside the path (i). The integration along the semicircular path in the upper omega plane,

Im $\omega > 0$, becomes zero in (A3). We then obtain $f(t) = 0$ for $t < 0$. For $t > 0$, we take the path (ii) for the integration and have

$$f(t) = 2\pi i[\mathrm{Res}(-\omega_0) + \mathrm{Res}(\omega_0) + \mathrm{Res}(0)] \text{ for } t > 0 \tag{A5}$$

where $\mathrm{Res}(\omega_0)$ means the residue at $\omega = \omega_0$. Calculating the residue values and considering that integration along the semicircular path in the lower omega plane, Im $\omega < 0$, yields zero, we obtain

$$f(t) = \frac{1}{\omega_0^2}(1 - \cos(\omega_0 t)) \text{ for } t > 0 \tag{A6}$$

Combining the results of $t < 0$ and $t > 0$, we get

$$\begin{aligned} f(t) &= \frac{1}{2\pi}\int_{-\infty}^{\infty} d\omega\, e^{-i\omega t}\frac{1}{\omega^2 - \omega_0^2}\frac{1}{i\omega} \\ &= \frac{1}{\omega_0^2}(1 - \cos(\omega_0 t))H(t) \end{aligned} \tag{A7}$$

where $H(t)$ is the step function: $H(t) = 1$ when $t > +0$ and $H(t) = 0$ when $t < -0$. Using Eq. (A7), we calculate the vertical displacement as

$$\begin{aligned} &u_z(x, y, z, t) \\ &= \frac{1}{(2\pi)^2}\iint_{-\infty}^{\infty} dk_x dk_y e^{i(k_x x + k_y y)}\frac{k^2}{\rho_0}\frac{\sinh[k(h_0 - z)]}{\cosh(kh_0)}\frac{p_0(k_x, k_y)}{k}\frac{1}{\omega_0^2}[1 \\ &\quad - \cos(\omega_0 t)]H(t) \\ &= \frac{1}{(2\pi)^2}\iint_{-\infty}^{\infty} dk_x dk_y e^{i(k_x x + k_y y)}\frac{p_0(k_x, k_y)}{\rho_0 g_0}\frac{\sinh[k(h_0 - z)]}{\sinh(kh_0)}[1 - \cos(\omega_0 t)]H(t) \end{aligned} \tag{A8}$$

where we used the dispersion relation $\omega_0 = \sqrt{g_0 k \tanh(kh_0)}$. This is the same as Eq. (28).

**Appendix B: Tsunami generation due to sea-bottom deformation**

Tsunami generation due to the sea bottom was described in past studies (e.g., Takahashi 1942), but most studies employed the spatial description (Euler description). This appendix derives the equations using the material description (Lagrange description) with the propagator matrix method. The 3-D linear momentum equation (Eq. (1)), stress tensor (Eq. (2)), and the incompressible equation (Eq. (3)) are the same as those used in the surface pressure change source.

$$\rho_0\frac{\partial^2 \mathbf{u}(x, y, z, t)}{\partial t^2} = \nabla \cdot \boldsymbol{\tau} + \rho_0 g_0[\nabla u_z - (\nabla \cdot \mathbf{u})\bar{\mathbf{e}}_z] \tag{B1}$$

$$\boldsymbol{\tau}(x,y,z,t) = -p(x,y,z,t)\mathbf{I} \tag{B2}$$

$$\nabla \cdot \mathbf{u} = 0 \tag{B3}$$

The boundary condition at the sea surface is

$$p(x,y,0,t) = 0. \tag{B4}$$

The vertical displacement at the sea bottom is given by

$$\begin{aligned} u_z(x,y,h_0,t) &= u_0(x,y)H(t) \\ &= \frac{1}{(2\pi)^2}\iint_{-\infty}^{\infty} dk_x dk_y \hat{u}\big(k_x,k_y\big)e^{i(k_x x + k_y y)}\,H(t) \end{aligned} \tag{B5}$$

for a sudden sea-bottom deformation.

Using the same procedure as for Eq. (14), we obtain

$$\begin{pmatrix} U_z\big(k_x,k_y,h_0,\omega\big) \\ T_z\big(k_x,k_y,h_0,\omega\big) \end{pmatrix} = \begin{pmatrix} A_{11}(h_0) & A_{12}(h_0) \\ A_{21}(h_0) & A_{22}(h_0) \end{pmatrix} \begin{pmatrix} U_z\big(k_x,k_y,0,\omega\big) \\ 0 \end{pmatrix}. \tag{B6}$$

where the matrix $\mathbf{A}(z)$ is the same as Eq. (12) and

$$U_z\big(k_x,k_y,h_0,\omega\big) = \frac{1}{-i\omega}\hat{u}\big(k_x,k_y\big). \tag{B7}$$

For example, we show the procedure for deriving the ocean-bottom pressure change $p(x,y,h_0,t)$**.**
Eq. (B6) gives

$$T_z\big(k_x,k_y,h_0,\omega\big) = \frac{A_{21}(h_0)}{A_{11}(h_0)}U_z\big(k_x,k_y,h_0,\omega\big). \tag{B8}$$

Using Eq. (6) and Eq. (B8), the pressure change at the sea bottom is

$$
\begin{aligned}
&p(x,y,h_0,t)\\
&= -\frac{1}{2\pi}\int_{\infty}^{\infty} d\omega\, e^{-i\omega t}\frac{1}{(2\pi)^2}\iint_{-\infty}^{\infty} dk_x dk_y \frac{A_{21}(h_0)}{A_{11}(h_0)} U_z\big(k_x,k_y,h_0,\omega\big)\, k e^{i(k_x x+k_y y)}\\
&= \frac{1}{(2\pi)^2}\iint_{-\infty}^{\infty} dk_x dk_y e^{i(k_x x+k_y y)}\rho_0 h\frac{\tanh(kh_0)}{kh_0}\frac{1}{2\pi}\int_{\infty}^{\infty} d\omega\, e^{-i\omega t}\left(\frac{i\omega^3}{\omega^2-\omega_0^2}\right.\\
&\qquad\qquad \left. -\frac{i}{\omega}\frac{g_0^2k^2}{\omega^2-\omega_0^2}\right)
\end{aligned}
\tag{B9}
$$

Using the residue theorem (see Appendix A), we calculate (B9). However, we should note that we cannot directly apply the residue theorem for the integral in

$$
g(t) = \frac{1}{2\pi}\int_{-\infty}^{\infty} d\omega\, e^{-i\omega t}\frac{i\omega^3}{\omega^2-\omega_0^2} \tag{B10}
$$

that appears in Eq. (B9), because integration along the semicircular path does not yield zero. Therefore, instead of Eq. (B9), we consider the integral:

$$
\frac{1}{2\pi}\int_{-\infty}^{\infty} d\omega\, e^{-i\omega t}\frac{1}{\omega^2-\omega_0^2}\frac{1}{i\omega} = \frac{1}{\omega_0^2}(1-\cos(\omega_0 t))H(t). \tag{B11}
$$

Note that we calculated this in Appendix A with the residue theorem. By differentiating the left-hand side of (B11) with respect to time twice, we obtain the left-hand side as

$$
\frac{1}{2\pi}\int_{-\infty}^{\infty} d\omega\, e^{-i\omega t}\frac{i\omega}{\omega^2-\omega_0^2} \tag{B12}
$$

and the right hand as

$$
\begin{aligned}
\frac{d^2}{dt^2}\left[\frac{1}{\omega_0^2}(1-\cos(\omega_0 t))H(t)\right] &= \frac{d}{dt}\left[\frac{1}{\omega_0}\sin(\omega_0 t)\,H(t) + \frac{1}{\omega_0^2}(1-\cos(\omega_0 t))\delta(t)\right]\\
&= \frac{d}{dt}\left[\frac{1}{\omega_0}\sin(\omega_0 t)\,H(t)\right]\\
&= \cos(\omega_0 t)\,H(t) + \frac{1}{\omega_0}\sin(\omega_0 t)\,\delta(t)\\
&= \cos(\omega_0 t)\,H(t)
\end{aligned}
\tag{B13}
$$

Therefore, we obtain

$$
\frac{1}{2\pi}\int_{-\infty}^{\infty} d\omega\, e^{-i\omega t}\frac{i\omega}{\omega^2-\omega_0^2} = \cos(\omega_0 t)\,H(t) \tag{B14}
$$

Again, we differentiate (B14) with respect to time twice and obtain

$$\begin{aligned}\frac{1}{2\pi}\int_{-\infty}^{\infty} d\omega\, e^{-i\omega t}\frac{-i\omega^3}{\omega^2-\omega_0^2} &= \frac{d^2}{dt^2}\left[\cos(\omega_0 t)\,H(t)\right]\\ &= \frac{d}{dt}\left[-\omega_0\sin(\omega_0 t)\,H(t)+\cos(\omega_0 t)\,\delta(t)\right]\\ &= \frac{d}{dt}\left[-\omega_0\sin(\omega_0 t)\,H(t)+\delta(t)\right]\\ &= -\omega_0^2\cos(\omega_0 t)\,H(t)-\omega_0\sin(\omega_0 t)\,\delta(t)+\frac{d\delta(t)}{dt}\\ &= -\omega_0^2\cos(\omega_0 t)\,H(t)+\frac{d\delta(t)}{dt}.\end{aligned} \tag{B15}$$

Hence, we obtain

$$\frac{1}{2\pi}\int_{-\infty}^{\infty} d\omega\, e^{-i\omega t}\frac{i\omega^3}{\omega^2-\omega_0^2} = \omega_0^2\cos(\omega_0 t)\,H(t)-\frac{d\delta(t)}{dt} \tag{B16}$$

Using (B11) and (B16), we calculate (B9) as

$$\begin{aligned}&p(x,y,h_0,t)\\ &= \frac{1}{(2\pi)^2}\iint_{-\infty}^{\infty} dk_x dk_y e^{i(k_x x+k_y y)}\left[-\frac{\rho g_0\hat{u}_0(k_x,k_y)}{(\cosh kh_0)^2}\cos(\omega_0 t)\,H(t)\right.\\ &\qquad\left.-\rho_0 h\frac{\tanh(kh_0)}{kh_0}\hat{u}_0(k_x,k_y)\delta'(t)+\rho_0 g_0\hat{u}_0(k_x,k_y)H(t)\right]\\ &= \frac{1}{(2\pi)^2}\iint_{-\infty}^{\infty} dk_x dk_y e^{i(k_x x+k_y y)}\left[-\frac{\rho_0 g_0\hat{u}_0(k_x,k_y)}{(\cosh kh_0)^2}\cos(\omega_0 t)\,H(t)\right.\\ &\qquad\left.-\rho_0 h\frac{\tanh(kh_0)}{kh_0}\hat{u}_0(k_x,k_y)\delta'(t)\right]+\rho_0 g_0 u_0(x,y)H(t).\end{aligned} \tag{B14}$$

The first term represents the loading from the sea-surface height, the second term represents the dynamic pressure change caused by the accelerating sea-bottom deformation, and the third term represents the hydrostatic pressure change due to the sea-bottom displacement. Similarly, using Eq. (B12), we obtain the sea-surface height

$$\begin{aligned}\eta(x,y,t) &= -u_z(x,y,0,t)\\ &= \frac{-1}{(2\pi)^2}\iint_{-\infty}^{\infty} dk_x dk_y e^{i(k_x x+k_y y)}\frac{\hat{u}_0(k_x,k_y)}{\cosh kh_0}\cos(\omega_0 t)\,H(t).\end{aligned} \tag{B15}$$

## References

Aki, K. & Richards, P., 2002. *Quantitative Seismology* (2nd ed.), University Science Books.

An, C., Liu, P. L. F., & Seo, S. N. (2012). Large-scale edge waves generated by a moving atmospheric pressure. *Theoretical and Applied Mechanics Letters*, *2*(4), 042001. https://doi.org/10.1063/2.1204201

Aoi, S., Asano, Y., Kunugi, T., Kimura, T., Uehira, K., Takahashi, N., et al. (2020). MOWLAS: NIED observation network for earthquake, tsunami and volcano. *Earth, Planets and Space*, *72*, 126. https://doi.org/10.1186/s40623-020-01250-x

Baba, T., Takahashi, N., Kaneda, Y., Ando, K., Matsuoka, D., & Kato, T. (2015). Parallel Implementation of Dispersive Tsunami Wave Modeling with a Nesting Algorithm for the 2011 Tohoku Tsunami. *Pure and Applied Geophysics*, *172*(12), 3455–3472. https://doi.org/10.1007/s00024-015-1049-2

Baba, T., Gon, Y., Imai, K., Yamashita, K., Matsuno, T., Hayashi, M., & Ichihara, H. (2019). Modeling of a dispersive tsunami caused by a submarine landslide based on detailed bathymetry of the continental slope in the Nankai trough, southwest Japan. *Tectonophysics*, *768*(July), 228182. https://doi.org/10.1016/j.tecto.2019.228182

Bernard EN, Meinig C. 2011. History and future of deep-ocean tsunami measurements. Ocean. MTS/IEEE KONA, pp. 1–7. IEEE

Churchill, D. D., Houston, S. H., & Bond, N. A. (1995). The Daytona Beach Wave of 3–4 July 1992: A Shallow-Water Gravity Wave Forced by a Propagating Squall Line. *Bulletin of the American Meteorological Society*, *76*(1), 21–32. https://doi.org/10.1175/1520-0477(1995)076<0021:TDBWOJ>2.0.CO;2

Dahlen, F. A., & Tromp, J. (1998). *Theoretical Global Seismology*. Princeton University Press.

Gilbert, F., & Backus, G. E. (1966). Propagation matrices in elastic wave and vibration problems. *Geophysics*, *31*, 326–332. https://doi.org/10.1190/1.1439771

Greenspan, H. P. (1956). The generation of edge waves by moving pressure distributions. *Journal of Fluid Mechanics*, *1*(06), 574. https://doi.org/10.1017/S002211205600038X

Grilli, S. T., Harris, J. C., Tajalli Bakhsh, T. S., Masterlark, T. L., Kyriakopoulos, C., Kirby, J. T., & Shi, F. (2013). Numerical Simulation of the 2011 Tohoku Tsunami Based on a New Transient FEM Co-seismic Source: Comparison to Far- and Near-Field Observations. *Pure and Applied Geophysics*, *170*(6–8), 1333–1359. https://doi.org/10.1007/s00024-012-0528-y

Heidarzadeh, M., Šepić, J., Rabinovich, A., Allahyar, M., Soltanpour, A., & Tavakoli, F. (2020). Meteorological Tsunami of 19 March 2017 in the Persian Gulf: Observations and Analyses. *Pure and Applied Geophysics*, *177*(3), 1231–1259. https://doi.org/10.1007/s00024-019-02263-8

Hibiya, T., & Kajiura, K. (1982). Origin of the Abiki phenomenon (a kind of seiche) in Nagasaki Bay. *Journal of the Oceanographical Society of Japan*, *38*(3), 172–182. https://doi.org/10.1007/BF02110288

Inazu, D., & Saito, T. (2014). Two subevents across the Japan Trench during the 7 December 2012 off Tohoku earthquake (Mw 7.3) inferred from offshore tsunami records. *J. Geophys. Res.*, *119*(7), 5800–5813. https://doi.org/doi:10.1002/2013JB010892

Kanazawa T, Uehira K, Mochizuki M, Shinbo T, Fujimoto H, Noguchi S, et al. 2016. S-net project, cabled observation network for earthquakes and tsunamis, Paper presented at SubOptic 2016, Dubai

Kaneda Y, Kawaguchi K, Araki E, Matsumoto H, Nakamura T, et al. 2015. Development and application of an advanced ocean floor network system for megathrust earthquakes and tsunamis. In Seafloor Observatories, ed. P. Favali et al., pp. 643–62. Berlin/Heidelberg: Springer

Kawaguchi K, Kaneko S, Nishida T, Komine T. 2015. Construction of the DONET real-time seafloor observatory for earthquakes and tsunami monitoring. In Seafloor Observatories, ed. P. Favali et al., pp. 211–28. Berlin/Heidelberg: Springer

Kirby, J. T., Shi, F., Tehranirad, B., Harris, J. C., & Grilli, S. T. (2013). Dispersive tsunami waves in the ocean: Model equations and sensitivity to dispersion and Coriolis effects. *Ocean Modelling*, *62*, 39–55. https://doi.org/10.1016/j.ocemod.2012.11.009

Kubota, T., Saito, T., & Suzuki, W. (2020a). Millimeter-Scale Tsunami Detected by a Wide and Dense Observation Array in the Deep Ocean: Fault Modeling of an Mw 6.0 Interplate Earthquake off Sanriku, NE Japan. *Geophysical Research Letters*, *47*(4), 1–11. https://doi.org/10.1029/2019GL085842

Kubota, T., Saito, T., Chikasada, N. Y., & Suzuki, W. (2020b). Ultra-broadband seismic and tsunami wave observation of high-sampling ocean-bottom pressure gauge covering periods from seconds to hours. *Earth and Space Science*. https://doi.org/10.1029/2020ea001197

Lotto, G. C., & Dunham, E. M. (2015). High-order finite difference modeling of tsunami generation in a compressible ocean from offshore earthquakes. *Computational Geosciences*, *19*(2), 327–340. https://doi.org/10.1007/s10596-015-9472-0

Lotto, G. C., Nava, G., & Dunham, E. M. (2017). Should tsunami simulations include a nonzero initial horizontal velocity? *Earth, Planets and Space*, *69*(1), 117. https://doi.org/10.1186/s40623-017-0701-8

Mikada, H., Mitsuzawa, K., Matsumoto, H., Watanabe, T., Morita, S., Otsuka, R., et al. (2006). New discoveries in dynamics of an M8 earthquake-phenomena and their implications from the 2003 Tokachi-oki earthquake using a long term monitoring cabled observatory. *Tectonophysics*, *426*(1–2), 95–105. https://doi.org/10.1016/j.tecto.2006.02.021

Maeda, T., & Furumura, T. (2013). FDM Simulation of Seismic Waves, Ocean Acoustic Waves, and Tsunamis Based on Tsunami-Coupled Equations of Motion. *Pure and Applied Geophysics*, *170*(1–2), 109–127. https://doi.org/10.1007/s00024-011-0430-z

Mizutani, A., Yomogida, K., & Tanioka, Y. (2020). Early tsunami detection with near-fault ocean-bottom pressure gauge records based on the comparison with seismic data at common sites Key Points : https://doi.org/10.1029/2020JC016275

Monserrat, S., Vilibić, I., & Rabinovich, A. B. (2006). Meteotsunamis: Atmospherically induced destructive ocean waves in the tsunami frequency band. *Natural Hazards and Earth System Science*, *6*(6), 1035–1051. https://doi.org/10.5194/nhess-6-1035-2006

Mungov, G., Eblé, M., & Bouchard, R. (2013). DART® Tsunameter Retrospective and Real-Time Data: A Reflection on 10 Years of Processing in Support of Tsunami Research and Operations. *Pure and Applied Geophysics*, *170*(9–10), 1369–1384. https://doi.org/10.1007/s00024-012-0477-5

Nosov, M. A., Kolesov, S. V., Denisova, A. V., Alekseev, A. B., & Levin, B. V. (2007). On the near-bottom pressure variations in the region of the 2003 Tokachi-Oki tsunami source. *Oceanology*, *47*(1), 26–32. https://doi.org/10.1134/s0001437007010055

Pedlosky, J. (2013). *Waves in the ocean and atmosphere: Introduction to wave dynamics*. Berlin: Springer Berlin. https://doi.org/10.1007/978-3-662-05131-3

Proudman, J. (1929). The Effects on the Sea of Changes in Atmospheric Pressure. *Geophysical Journal International*, *2*(1926), 197–209. https://doi.org/10.1111/j.1365-246X.1929.tb05408.x

Rabinovich, A. B., & Eblé, M. C. (2015). Deep-Ocean Measurements of Tsunami Waves. *Pure and Applied Geophysics*, *172*, 3281–3312. https://doi.org/10.1007/s00024-015-1058-1

Rabinovich, A. B., Šepić, J., & Thomson, R. E. (2020). *The meteorological tsunami of 1 November 2010 in the southern Strait of Georgia: a case study*. *Natural Hazards*. Springer Netherlands. https://doi.org/10.1007/s11069-020-04203-5

Saito, T. (2019). *Tsunami Generation and Propagation. Springer*.

Saito, T. (2013). Dynamic tsunami generation due to sea-bottom deformation: Analytical representation based on linear potential theory. *Earth, Planets and Space*, *65*(12), 1411–1423. https://doi.org/10.5047/eps.2013.07.004

Saito, T., & Furumura, T. (2009). Three-dimensional tsunami generation simulation due to sea-bottom deformation and its interpretation based on the linear theory. *Geophysical Journal International*, *178*(2), 877–888. https://doi.org/10.1111/j.1365-246X.2009.04206.x

Saito, T., Inazu, D., Miyoshi, T., & Hino, R. (2014). Dispersion and nonlinear effects in the 2011 Tohoku-Oki earthquake tsunami. *Journal of Geophysical Research: Oceans*. https://doi.org/10.1002/2014JC009971

Saito, T., & Tsushima, H. (2016). Synthesizing ocean bottom pressure records including seismic wave and tsunami contributions: Toward realistic tests of monitoring systems. *Journal of Geophysical Research: Solid Earth*, *121*(11), 8175–8195. https://doi.org/10.1002/2016JB013195

Saito, T., Baba, T., Inazu, D., Takemura, S., & Fukuyama, E. (2019). Synthesizing sea surface height change including seismic waves and tsunami using a dynamic rupture scenario of anticipated Nankai trough earthquakes. *Tectonophysics*, *769*(July), 228166. https://doi.org/10.1016/j.tecto.2019.228166

Saito, T., & Kubota, T. (2020). Tsunami modeling for the deep sea and inside focal areas. *Annual Review of Earth and Planetary Sciences*, *48*, 121–145. https://doi.org/10.1146/annurev-earth-071719-054845

Sandanbata, O., Watada, S., Satake, K., Fukao, Y., Sugioka, H., Ito, A., & Shiobara, H. (2018). Ray tracing for dispersive tsunamis and source amplitude estimation based on Green's law: Application to the 2015 volcanic tsunami earthquake near Torishima, south of Japan. *Pure and Applied Geophysics*, *175*(4), 1371–1385. https://doi.org/10.1007/s00024-017-1746-0

Segall, P. (2010). *Earthquake and volcano deformation*. Princeton: Princeton University Press. https://doi.org/10.1515/9781400833856

Seo, S. N., & Liu, P. L. F. (2014). Edge waves generated by atmospheric pressure disturbances moving along a shoreline on a sloping beach. *Coastal Engineering*, *85*, 43–59. https://doi.org/10.1016/j.coastaleng.2013.12.002

Šepić, J., Vilibić, I., Rabinovich, A. B., & Monserrat, S. (2015). Widespread tsunami-like waves of 23-27 June in the Mediterranean and Black Seas generated by high-altitude atmospheric forcing. *Scientific Reports*, *5*(1), 11682. https://doi.org/10.1038/srep11682

Takahashi, R., On seismic sea waves caused by deformations of the sea bottom, Bull. Earthq. Res. Inst., 20, 357–400, 1942 (in Japanese with English abstract).

Tsushima, H., & Ohta, Y. (2014). Review on near-field tsunami forecasting from offshore tsunami data and onshore GNSS data for tsunami early warning. *Journal of Disaster Research*, *9*(3), 339–357. https://doi.org/10.20965/jdr.2014.p0339

Williams, D. A., Horsburgh, K. J., Schultz, D. M., & Hughes, C. W. (2019). Examination of generation mechanisms for an english channel meteotsunami: Combining observations and modeling. *Journal of Physical Oceanography*, *49*(1), 103–120. https://doi.org/10.1175/JPO-D-18-0161.1

**Acknowledgments, Samples, and Data**

This study is supported by Japan Society for the Promotion of Science (JSPS) KAKENHI Grant Numbers 19H02409. This study does not use observed data. All the results are derived from the equations derived in this study.